



## REVIEW

[View Article Online](#)  
[View Journal](#) | [View Issue](#)Cite this: *Mater. Horiz.*, 2025,  
12, 4042Innovative materials that behave like robots to  
combat plastic pollutionShafqat Ali, <sup>a</sup> Muhammad Haris Khan,<sup>b</sup> Zareen Zuhra <sup>\*b</sup> and Jinfeng Wang<sup>\*a</sup>

The growing plastic pollution crisis demands novel approaches, with innovative materials that mimic robotic behaviors emerging as a promising solution. This approach explores the development and application of smart materials that can autonomously engage in plastic waste removal, functioning like robots under various environmental conditions. We focus on materials activated by light, magnetic fields, chemical fuels, and ion exchange, which are designed to target and remove plastic waste efficiently. The key properties of these materials, such as self-activation, adaptability, and precision that enable them to function autonomously in waste management systems, are examined. The integration of these innovative materials offers significant advantages, including faster waste processing, reduced human exposure to hazardous waste, and enhanced sorting accuracy. Additionally, this review evaluates the environmental impact, scalability, and cost-effectiveness of these materials in comparison to traditional methods. Finally, the potential of these materials to play a central role in sustainable plastic waste management and contribute to a circular economy is discussed.

Received 6th December 2024,  
Accepted 14th March 2025

DOI: 10.1039/d4mh01772b

[rsc.li/materials-horizons](https://rsc.li/materials-horizons)

## Wider impact

This review highlights key advancements in the development of innovative materials that mimic robotic behaviors for plastic waste removal. Key developments include the use of materials activated by light, magnetic fields, chemical fuels, and ion exchange, which can autonomously target, collect, and sort plastic waste. These materials represent a new frontier in waste management, offering a more efficient, scalable, and sustainable solution compared to traditional methods. This area is of significant wider interest due to the urgent global need to address plastic pollution, which poses serious environmental, ecological, and public health risks. By leveraging advanced materials science, these robotic materials can revolutionize the way we manage plastic waste, reduce human exposure to hazardous waste, and contribute to the broader goals of a circular economy. The future of this field promises increasingly intelligent, adaptive materials capable of performing complex tasks autonomously in diverse environments. The insights from this review will shape materials science by advancing our understanding of smart, self-acting materials and their integration into real-world applications, driving innovation in both waste management and sustainable materials design.

## 1. Introduction

Plastic, a versatile and durable polymeric material, was first developed in the early 20th century.<sup>1</sup> It revolutionized many industries due to its unique features like light weight, moldability, and low production cost.<sup>2</sup> The first completely synthetic plastic, Bakelite, was formed by Leo Baekeland in 1907.<sup>3</sup> Since then, the production and use of plastics have exponentially increased, leading to their ubiquitous presence in everyday life.<sup>4</sup> Plastics are used in a wide range of products, including

packaging, household items, medical devices and construction materials.<sup>5</sup> Global plastic production has skyrocketed from 2 million metric tons in 1950 to over 400 million metric tons in 2020, with around 14 million tons of plastic waste entering water systems each year.<sup>6</sup> This surge in production has led to a substantial increase in plastic waste. The United Nations Environment Program (UNEP) reports that approximately 300 million tons of plastic waste are generated annually.<sup>7</sup> Microplastics (MPs), which are plastic particles smaller than 5 millimeters, and nanoplastics (NPs), even tinier at less than 100 nm,<sup>8</sup> present serious environmental and health risks due to their small size and persistence in ecosystems.<sup>9</sup> MPs often settle on the seafloor, while NPs, due to their buoyancy, remain suspended in water and spread quickly with ocean currents.<sup>10</sup> The overall journey of plastic to the human body is presented in Fig. 1(a),<sup>11</sup> while the chemical composition of plastic is

<sup>a</sup> State Key Laboratory of New Textile Materials and Advanced Processing Technologies, National Local Joint Laboratory for Advanced Textile Processing and Clean Production, Wuhan Textile University, Wuhan 430200, China.  
E-mail: [jinfeng.wang@wtu.edu.cn](mailto:jinfeng.wang@wtu.edu.cn)

<sup>b</sup> School of Bioengineering and Health, Wuhan Textile University, Wuhan 430200, P. R. China. E-mail: [zareenzuhraqau@gmail.com](mailto:zareenzuhraqau@gmail.com)

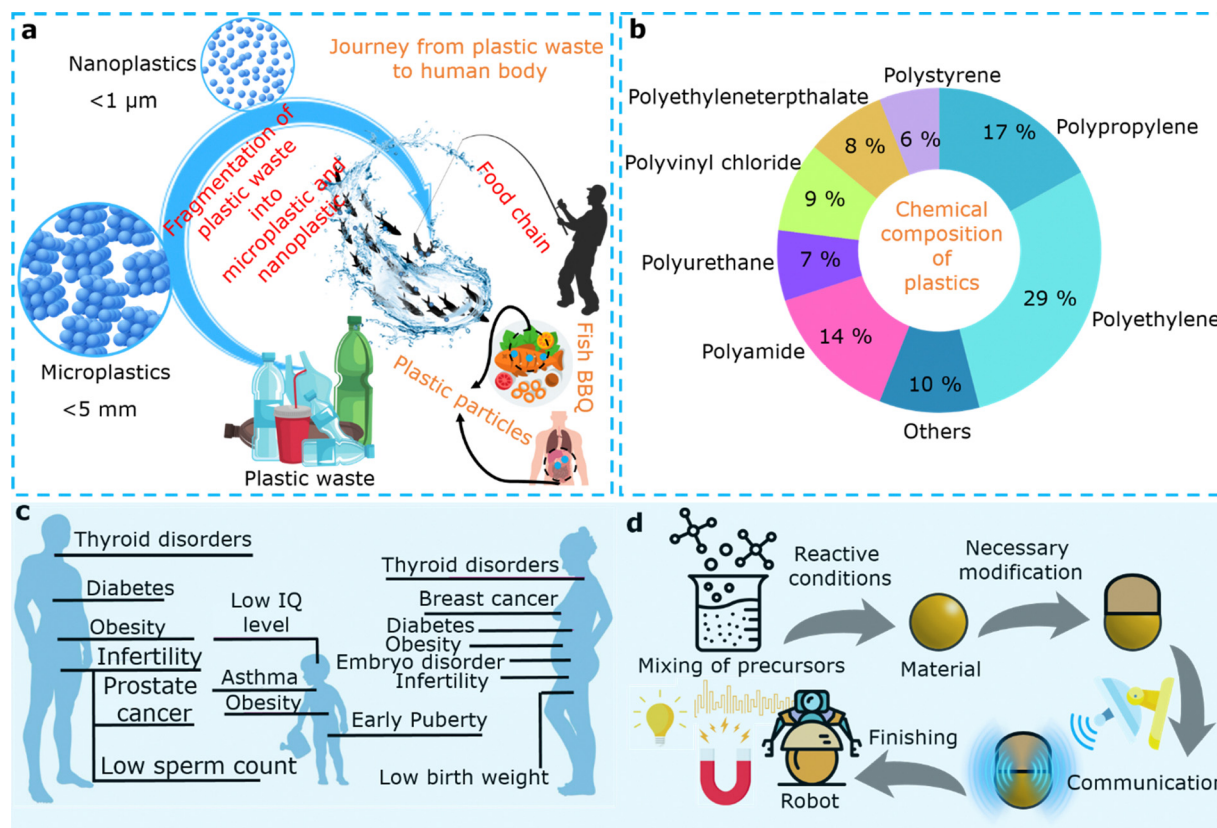


Fig. 1 The transportation of micro- and nanoplastics into the human body via the food chain (a). Adapted from ref. 11 Copyright 2022, Wiley-VCH. The chemical composition of plastic (b). Adapted from ref. 12 Copyright 2022, Elsevier. The adverse impact of plastic on human health (c). Adapted from ref. 17 Copyright 2019, Island Press. The route for converting materials into robots (d). Adapted from ref. 19 Copyright 2023, Springer Nature.

summarized in Fig. 1(b).<sup>12</sup> Ingestion of plastics, including micro- and nanoplastics (MNPs), by aquatic organisms can lead to various health issues, such as physical harm and blockages in the digestive tract.<sup>13</sup> Additionally, MNPs can negatively impact the behavior and reproductive health of these organisms.<sup>14</sup> Although the full impact of MNPs on human health is not yet fully understood,<sup>15</sup> recent studies have indicated that these particles can be transferred through the food chain (Fig. 1(a)) and accumulate in human tissues.<sup>16</sup> This accumulation may result in a range of health problems, including inflammation, genetic damage, and even cancer (Fig. 1(c)).<sup>17</sup> As a result, pollution caused by MNPs has become an increasingly urgent concern, emphasizing the need for innovative strategies to effectively capture, concentrate, and remove these plastic particles.<sup>18</sup>

Effectively treating large volumes of water contaminated with MNPs involves addressing several challenges.<sup>20</sup> These include removing ultra-small particles, achieving high removal efficiency even at low MNP concentrations in the environment, and treating large amounts of wastewater at a low cost.<sup>21</sup> Traditional methods, such as physical adsorption, filtration, biological ingestion, and chemical treatments, have been employed to tackle these issues.<sup>22,23</sup> However, each approach has its own advantages and drawbacks that must be carefully considered.<sup>24</sup> For instance, while filtration can achieve high removal efficiency, its high energy consumption and potential

nanoplastic filtering losses hinder large-scale application.<sup>25,26</sup> Chemical flocculation offers a low-energy alternative, but it has limited removal capacity and the potential to cause secondary pollution.<sup>27</sup> Biological treatment, though environmentally friendly, is only suitable under specific conditions and has a slower removal rate.<sup>28</sup> Therefore, finding an optimal solution requires balancing the trade-offs between removal efficiency, cost, and environmental impact.

The advent of micro- and nanorobots (MNRs) represents a remarkable integration of robotics, materials science and nanotechnology.<sup>29</sup> These tiny robots, often ranging in size from micrometers to nanometers, leverage the distinct physical and chemical properties of micro- and nanomaterials to execute tasks with remarkable precision.<sup>30</sup> By integrating these materials with advanced locomotion and positional control mechanisms, MNRs are transforming a multitude of application domains, including biomedicine,<sup>31</sup> sensing,<sup>32</sup> imaging<sup>33</sup> and environmental remediation.<sup>19</sup> MNRs leverage the exceptional attributes of their constituent materials, such as a high surface area-to-volume ratio, enhanced mechanical strength, and tailored chemical reactivity.<sup>34</sup> These properties enable them to interact effectively with their surroundings, making them ideal for applications requiring delicate handling or targeted actions.<sup>35</sup> The locomotion of these robots can be controlled through various mechanisms like magnetic fields for remote

control,<sup>36,37</sup> chemical reactions for propulsion,<sup>38</sup> optical methods<sup>39</sup> like lasers for precise movement and mechanical systems that utilize cilia or flagella.<sup>40</sup> The introduction of mutual communication can transform micro- and nanomaterials into intelligent micro- and nanorobots (Fig. 1(d)).<sup>19</sup> In biomedicine, MNRs offer transformative potential.<sup>41</sup> They can be employed for targeted drug delivery, ensuring that medications are administered directly to specific cells or tissues, thereby minimizing side effects and enhancing treatment efficacy.<sup>42</sup> Additionally, they are useful in diagnostics, providing highly sensitive detection of biomarkers.<sup>43</sup> Their precision also makes them valuable in minimally invasive surgical procedures, where they can perform delicate operations with high accuracy.<sup>44</sup> For sensing and imaging, MNRs provide advanced capabilities.<sup>45</sup> They can monitor environmental conditions in real-time, detecting pollutants and hazardous chemicals with high sensitivity.<sup>30</sup> In medical imaging, these robots improve the resolution and detail of images, significantly aiding in the diagnosis and treatment of various conditions.<sup>45</sup>

Recently, the promising applications of MNRs in environmental remediation, particularly in addressing the issue of MNPs, have gained attention.<sup>19</sup> These robots can be designed to detect and neutralize plastic pollutants at a molecular MNP level.<sup>46</sup> Some are equipped to break down MPs into less harmful substances,<sup>47</sup> while others can collect and concentrate these particles for easier removal.<sup>48</sup> Continuous monitoring by these robots also provides valuable data on plastic pollution, aiding in the management and mitigation of environmental damage.<sup>49,50</sup>

Ongoing research focuses on scaling production, increasing functionality, and addressing safety and ethical concerns to fully realize the potential of MNRs. Recent advancements have significantly improved the capabilities of MNRs. Innovative actuation methods, including new techniques for light, magnetic, and chemical control, have expanded their functional applications. The development of advanced materials and improved integration with existing technologies have enhanced their practical utility. This review covers the design principles and technological characteristics of MNRs, evaluates their current advancements and challenges in removing MNPs, and suggests directions for future research.

Robotic materials offer several advantages, including self-adaptability to changing environmental conditions and enhanced efficiency in applications such as environmental remediation, precision manufacturing, and medical devices.<sup>51</sup> Their multifunctional nature reduces system complexity and increases design flexibility. Furthermore, robotic materials have the potential for scalability, enabling their use in large-scale applications like environmental monitoring and autonomous infrastructure repair.<sup>52</sup> However, there are certain limitations, including high development costs, complex maintenance requirements, and durability issues, particularly in harsh environments. Additionally, active robotic systems often require significant energy, which can hinder their widespread adoption.<sup>53</sup> Despite these challenges, robotic materials have demonstrated practical applications in diverse fields, such as environmental remediation through

autonomous pollutant detection and degradation, smart prosthetics and wearable sensors for improved healthcare, infrastructure monitoring for self-repair, and manufacturing automation for enhanced production efficiency.<sup>54</sup> In search-and-rescue operations, the use of robotic materials in soft robotics has proven invaluable, where traditional rigid materials are unsuitable.<sup>55</sup> This review's comprehensive analysis of smart materials for sustainable plastic remediation and the discussion of the advantages, limitations, and applications of robotic materials underscore their relevance and importance in advancing sustainable and technological innovations across multiple sectors.

## 2. Conventional methods for plastic removal

Various conventional methods for plastic removal have been employed over the years, each playing a crucial role in the fight against plastic waste.<sup>56</sup> Manual cleanup efforts (Fig. 2(a)) are among the most straightforward and widely used methods.<sup>57</sup> Community cleanups and organized events, such as International Coastal Cleanup Day, mobilize large groups of people to pick up litter, raising public awareness and engaging communities in environmental stewardship.<sup>58</sup> Mechanical collection, another key method (Fig. 2(b)), involves using machines like street sweepers to collect litter from urban areas and beach cleaning machines that sift sand to remove debris.<sup>59</sup> In aquatic environments, mechanical skimmers and booms are used to gather floating plastic waste from rivers, lakes, and harbors, though these devices often require significant maintenance and operational costs.<sup>60</sup> Trash traps and barriers are designed to capture plastic waste before it enters larger bodies of water, with structures typically installed in storm drains, river mouths, or along coastlines to intercept debris.<sup>12</sup> Examples include floating booms that funnel plastic waste into collection points and trash traps placed in drainage systems.<sup>61,62</sup> While effective in preventing plastic from reaching the ocean, these solutions depend on regular maintenance and the ability to handle large volumes of waste during heavy rainfalls.<sup>63,64</sup>

Various traditional methods have been developed to eliminate microplastic nanoparticles from water, and these methods can be broadly divided into physical,<sup>68</sup> chemical,<sup>69</sup> and biotechnological approaches.<sup>70</sup> Physical techniques generally include processes like filtration,<sup>71</sup> adsorption<sup>72</sup> and screening.<sup>73</sup> An example of a filtration device commonly used in wastewater treatment is the disc filter (Fig. 2(c)).<sup>65</sup> This device features several layers of overlapping filter screens and flange rings that capture microplastic debris as the wastewater flows through.<sup>74</sup> Notably, disc filters with pore sizes of 10 and 20  $\mu\text{m}$  have demonstrated the ability to remove approximately 89.7% of microplastic particles from water. In addition to physical filtration, advanced materials such as metal-organic frameworks (MOFs) are being explored for microplastic removal. These materials are characterized by their interpenetrating pores, high uniformity, and excellent durability. For instance, a zirconium-based MOF filter has been shown to





Fig. 2 Manual cleanup efforts for plastic removal near a river area (a). Adapted from ref. 57 Copyright 2021, Springer. Mechanical collection of plastic (b). Adapted from ref. 59 Copyright 2017, Sage. A setup of a disc filter for MP removal in wastewater (c). Adapted from ref. 65 Copyright 2019, MDPI. Zirconium MOF based filter and automatic filtration system for MP removal (d). Adapted from ref. 66 Copyright 2020, the Royal Society of Chemistry. Surface adsorption of plastics on  $\text{Fe}_3\text{O}_4$  (e). Adapted from ref. 67 Copyright 2022, Elsevier.

remove about 95.5% of microplastic particles from water. Furthermore, a lab-scale automatic filtration system has been developed that utilizes sunlight to power the water filtration process, offering a sustainable solution for microplastic removal (Fig. 2(d)).<sup>66</sup> Innovative adsorbents are being developed to enhance physical adsorption techniques. For example, magnetic ferric oxide ( $\text{Fe}_3\text{O}_4$ ) nanoparticles<sup>67</sup> have shown an impressive 80% efficiency in removing MPs such as polypropylene (PP), polystyrene (PS), and polyethylene (PE) microspheres by adsorbing them onto the  $\text{Fe}_3\text{O}_4$  surface. The adsorption of microplastics by magnetic iron oxide ( $\text{Fe}_3\text{O}_4$ ) nanoparticles is based on surface interactions, electrostatic attraction, and magnetic properties, which enable efficient separation from aqueous environments (Fig. 2(e)).<sup>67</sup> These nanoparticles possess a high surface area and abundant surface-active sites, including hydroxyl groups ( $-\text{OH}$ ) that play a crucial role in adsorption by forming hydrogen bonds or electrostatic interactions with microplastic

particles. The efficiency of adsorption is influenced by factors such as the surface charge of the nanoparticles, solution pH, and the characteristics of the microplastics, including their size, surface chemistry, and polarity.<sup>75</sup> Electrostatic interactions are a key mechanism in the adsorption process. Depending on the pH of the solution,  $\text{Fe}_3\text{O}_4$  nanoparticles can acquire a positive or negative surface charge. Microplastics, due to environmental aging and surface functionalization, also carry surface charges. When the charges are opposite, strong electrostatic attraction enhances the adhesion of microplastics to the nanoparticles. In addition to electrostatic forces, hydrophobic interactions further contribute to adsorption, as microplastics are primarily hydrophobic and can readily attach to  $\text{Fe}_3\text{O}_4$  nanoparticles, which may exhibit both hydrophobic and hydrophilic surface properties depending on surface modifications.<sup>76</sup> After adsorption, the magnetic properties of  $\text{Fe}_3\text{O}_4$  nanoparticles allow for the rapid and energy-efficient separation of

the nanoparticle–microplastic complex from water using an external magnetic field. This magnetic separation provides a sustainable and environmentally friendly approach for recovering microplastics along with the nanoparticles. To further enhance adsorption capacity and selectivity, surface modifications of  $\text{Fe}_3\text{O}_4$  nanoparticles can be employed, such as functionalization with organic polymers, surfactants, or inorganic materials.<sup>77</sup> These modifications improve the affinity for specific types of microplastics and increase the stability and dispersibility of the nanoparticles in water. In conclusion, the adsorption of microplastics by  $\text{Fe}_3\text{O}_4$  nanoparticles is a promising solution for environmental remediation, leveraging surface interactions and magnetic separation for effective microplastic removal from aquatic systems. Additionally, a composite material known as magnetic polyoxometalate-supported ionic liquid phase (magPOM-SILP) has been found to completely eliminate PS microplastics (at a concentration of  $1 \text{ g L}^{-1}$ ).<sup>78</sup> This is achieved through hydrophobic interactions between the POM-IL coating and the PS particles.

Coagulation and flocculation are essential chemical techniques used in wastewater treatment, where coagulants are added to promote strong interactions between particles.<sup>27</sup> Coagulation works by neutralizing particle charges, while flocculation involves the aggregation of particles through ligand exchange mechanisms.<sup>79</sup> Common coagulants for removing MPs from water include iron, aluminum, and polyamine-based compounds. To enhance the effectiveness of microplastic removal, anionic polyacrylamide (at concentrations of  $3\text{--}15 \text{ mg L}^{-1}$ ) is often combined with iron-based salts.<sup>80</sup> This combination has been shown to boost removal efficiency from 15% to 90.9%. The improvement is primarily due to the increased density of flocs when anionic polyacrylamide is added, which facilitates the adsorption and capture of microplastic particles.<sup>81</sup> As a result, polyacrylamide plays a critical role in improving the coagulation process and significantly increasing the efficiency of microplastic removal.

In contrast to physical and chemical methods, microorganisms offer a unique approach by breaking down MPs into smaller, more biodegradable components.<sup>82,83</sup> Some of the most commonly found plastics, including PE, PP, and PS, have been shown to degrade effectively through biological processes.<sup>84</sup> For example, Antarctic krill (*Euphausia superba*) have demonstrated the ability to fragment MPs (31.5 mm) into particles smaller than 1 mm, suggesting a biological pathway for converting MPs into NPs.<sup>85</sup> Additionally, certain bacteria, such as *Ideonella sakaiensis*, which has been isolated from mealworm guts and environments with polyethylene terephthalate (PET), have been identified as active agents in breaking down PET.<sup>86</sup> Although traditional methods for plastic removal whether physical, chemical, or biological are vital for reducing and eliminating plastic waste, their effectiveness diminishes when dealing with MNPs due to the minute sizes and low concentrations of these particles.<sup>87</sup> To address this challenge, future strategies may involve integrating traditional techniques with emerging nanotechnologies. This combination could enhance the ability to treat MNPs, thereby reducing their

environmental impact and contributing to more effective plastic waste management.<sup>88</sup>

### 3. Potential of robotic technology for plastic removal

The transition from traditional methods to robotic approaches represents a significant shift across various industries, driven by the need for enhanced efficiency, adaptability, and precision.<sup>89</sup> Traditional methods often rely on static processes and manual interventions, which can be time-consuming, error-prone, and inefficient in dynamic environments. In contrast, robotic solutions offer self-adaptability, automation, and real-time decision-making capabilities. They integrate sensing, actuation, and computation within a single system, enabling intelligent responses to environmental changes without human intervention.<sup>90</sup> This transition is evident in fields such as manufacturing, healthcare, environmental monitoring, and infrastructure maintenance. Robotic approaches not only reduce human workload but also enhance safety by taking on tasks in hazardous environments. Their ability to handle complex operations autonomously leads to greater productivity and cost savings over time.<sup>91</sup> Additionally, advancements in materials science have contributed to the development of robotic materials, further expanding their application potential. These materials are designed to mimic biological functions, making them ideal for soft robotics and adaptive systems. Overall, robotic solutions present unique advantages, including greater operational flexibility, improved accuracy, and reduced resource consumption, positioning them as transformative tools in the move toward smarter, more sustainable technologies.<sup>92</sup> Therefore the need for innovative and efficient removal strategies for MNPs is critical, and among the various approaches being explored, the deployment of robotic technologies stands out for its potential to revolutionize to tackle plastic pollution.<sup>50,92</sup> Robotic technologies for plastic removal utilize cutting-edge developments in artificial intelligence (AI), machine learning, sensor systems, and autonomous navigation.<sup>48,93</sup> These innovations enable robots to identify, remove, collect, and process plastic waste in diverse environments, making them highly effective in addressing the plastic pollution crisis.<sup>94</sup> Aquatic robots, such as The Ocean Cleanup Interceptors and Seabins, are designed to operate in water bodies, autonomously navigating through rivers, lakes, and oceans to collect plastic waste.<sup>60,95</sup> These robots use sensors and imaging technologies to detect and differentiate between plastic and other debris, ensuring efficient collection. The Ocean Cleanup project, for instance, has developed a system that captures plastic waste from ocean gyres and rivers, demonstrating significant potential in large-scale cleanups.<sup>96</sup> On land, robots like BeachBot, developed by a team from Delft University of Technology, are specifically designed to pick up small pieces of plastic waste on beaches.<sup>97</sup> These robots utilize AI algorithms to detect and identify plastic waste, ensuring precise and targeted removal. In industrial settings, robots are being used in waste management facilities to sort and process plastic waste

more efficiently than human workers.<sup>98</sup> Aerial drones equipped with cameras and sensors are also being used for surveillance and monitoring of plastic pollution.<sup>99</sup> These drones can cover large areas quickly, providing real-time data on the location and extent of plastic waste.<sup>100</sup> In some cases, drones are being developed to collect lightweight plastic debris, particularly in hard-to-reach areas such as remote shorelines and dense forests.<sup>101</sup> The deployment of robots for plastic removal offers several significant advantages over traditional methods. Robots can operate continuously and autonomously, significantly increasing the efficiency of plastic removal efforts. They can cover large areas and collect substantial amounts of plastic waste in a shorter time compared to manual cleanup efforts.<sup>102</sup> For instance, The Ocean Cleanup Interceptors can extract up to 50 000 kg of plastic waste per day from rivers, showcasing the scalability and effectiveness of robotic solutions.<sup>60</sup> Plastic cleanup, especially in aquatic environments, can be hazardous and labor-intensive. Robots can perform these tasks without risking human health and safety, making them ideal for operations in polluted and hazardous areas. This reduction in human labor also lowers the overall cost of cleanup operations. Robots can work around the clock without the need for rest, significantly enhancing the productivity of cleanup efforts.<sup>103</sup>

These micro- and nanomachines can transform different types of energy—such as ultrasound, light, electricity, heat, and magnetic energy—into mechanical motion, allowing them to operate effectively at micro and nanoscale levels within complex environments. The autonomous movement of these machines enhances their ability to interact with pollutants, speeding up the removal process and making them a powerful tool for water pollution remediation. Additionally, their small size enables them to maneuver through narrow channels and access areas that larger devices cannot reach.<sup>104</sup>

### 3.1. Light-powered robots for plastic removal

Photo-catalytic technology is recognized as an effective and safe method for environmental purification, earning acclaim from the international academic community for its ability to enhance pollutant treatment.<sup>105</sup> Common semiconductor photocatalysts, such as TiO<sub>2</sub>, ZnO, BiOCl, WO<sub>3</sub>, and g-C<sub>3</sub>N<sub>4</sub>, are often used to degrade MPs under light irradiation.<sup>106</sup> The fundamental principle behind photocatalysis involves the generation of photogenerated electrons (e<sup>-</sup>) and holes (h<sup>+</sup>) when the photocatalyst is exposed to light. These electrons and holes then react with adsorbed O<sub>2</sub>, H<sub>2</sub>O, and surface hydroxyl groups to produce reactive oxygen species, such as •O<sub>2</sub> and •OH.<sup>107</sup> These highly reactive species can initiate non-selective oxidation–reduction reactions with most organic molecules, leading to their complete mineralization into CO<sub>2</sub>, H<sub>2</sub>O, mineral acids, or salts.<sup>108</sup> Due to their exceptional photochemical activity, photo-catalytic materials are widely used in the design of light-driven micro/nanorobots (LMNRs).<sup>47</sup> These LMNRs can operate through various mechanisms, including self-electrophoresis, self-diffusiophoresis, and bubble propulsion.<sup>14</sup> In self-electrophoresis, the spatial separation of anodic and cathodic reactions creates an uneven charge distribution and a

propulsive electric field. On the other hand, self-diffusiophoresis occurs when anodic and cathodic reactions overlap spatially, generating different ion species on the same side of the MNR.<sup>30</sup> As these ions diffuse outward at varying rates, a concentration gradient forms, creating an electric field that propels the MNR. Bubble propulsion is achieved by creating bubble reactions, such as the splitting of H<sub>2</sub>O<sub>2</sub>, which drives the LMNR forward. Light serves as a versatile energy source and can also be used as an encoding signal, offering additional control over the LMNR movement.<sup>109</sup> Due to their biocompatibility, efficiency, and precision, LMNRs have gained widespread application in biomedical devices, environmental remediation, and smart assembly. In particular, LMNRs have been extensively researched for their potential in environmental cleanup efforts.<sup>110,111</sup>

Zhang and colleagues<sup>112</sup> developed Janus Au/WO<sub>3</sub>@C micro-robots that demonstrate improved mobility by utilizing photo-catalytic decomposition of organic materials when exposed to UV light. Similarly, AgCl microstar-based microrobots can degrade organic molecules and eliminate bacteria like “*Escherichia coli*” through light-driven propulsion.<sup>113</sup> Silver nanoparticles are crucial to this antibacterial process, and the autonomous movement of the microrobots enhances the dispersion of these nanoparticles, increasing their contact with bacteria and thus improving their bactericidal effectiveness. The phoretic interactions of LMNRs can be strategically engineered to offer distinct advantages in clustering, adsorption, and cargo transportation.<sup>114</sup> For instance, BiVO<sub>4</sub> microrobots powered by photocatalysis have shown the ability to load and transport passive particles as well as live microorganisms. These microrobots generate highly reactive oxygen species (ROS) through photo-catalytic reactions, which are effective in killing bacteria. Such multifunctional microrobots are promising for various applications, including cargo transport and the treatment of microbial contamination in water. Additionally, their ability to cluster and capture particles has significant potential for removing MPs, as large-scale aggregation and adsorption could greatly improve the efficiency of collecting micro- and nanoplastic particles.<sup>115</sup>

Ullattil and Pumera<sup>116</sup> introduced an innovative approach to creating asymmetric, single-component TiO<sub>2</sub> microrobots with a distinctive surface morphology transformation process that allows for phototrapping and photofragmenting MPs in water (Fig. 3(a)). These microrobots, which are rod-shaped and feature various trapping sites, are produced in a single reaction. Their asymmetrical design enhances propulsion, enabling them to work together efficiently to capture and break down MPs through photocatalysis. This model showcases a “unity in diversity” concept, where microrobots synergize to trap and fragment MPs under light exposure. When exposed to light, the surface morphology of these microrobots evolves into porous, flower-like structures that effectively capture MPs for degradation. In the presence of H<sub>2</sub>O<sub>2</sub>, the microrobots exhibit pronounced expansion and schooling behavior (Fig. 3(b)). Under UV light, the microrobot cluster initially expands, and when the light is switched off after 7 s, the cluster contracts and nearly



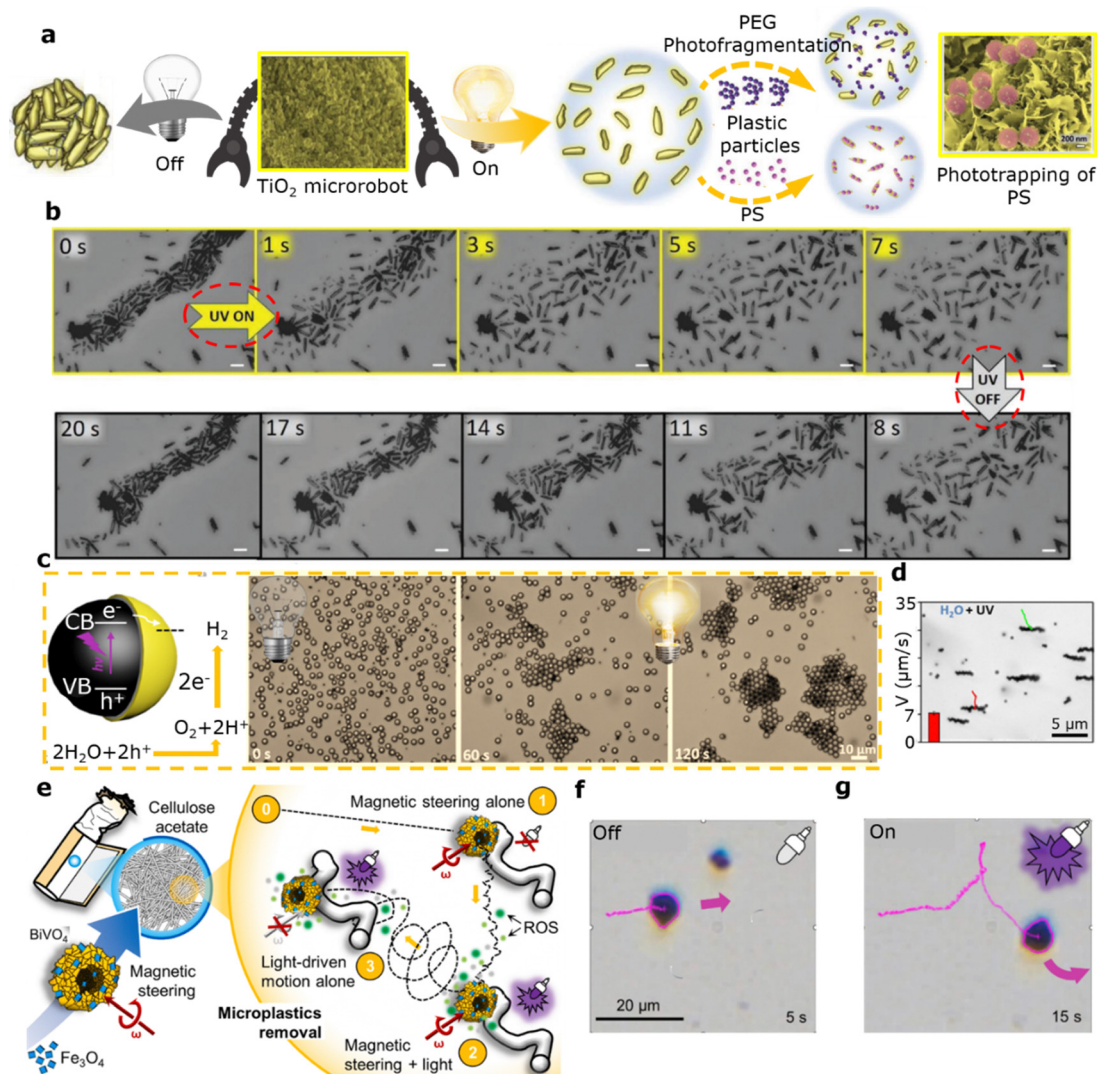


**Fig. 3** An overview of the general procedure of employing super-structured  $\text{TiO}_2$  microrobots to phototrap and photofragment MPs (a) and the growth and shrinkage of  $\text{TiO}_2$  microrobots with 0.5%  $\text{H}_2\text{O}_2$  and UV on/off conditions (b). Adapted from ref. 116 Copyright 2023, Wiley-VCH. The scale bar shows 10  $\mu\text{m}$ . Interaction of  $\text{Au@Ni@TiO}_2$  micromotor with PS particles (c) and showing the speed and track lines of the  $\text{Au@Ni@TiO}_2$  micromotor (d)<sup>117</sup> Copyright 2019, the American Chemical Society. The microrobot magnetic paths change (e) and (f)<sup>118</sup> Copyright 2023, Elsevier.

returns to its original form within 20 s. Before UV exposure, PS particles are loosely held at various sites such as cracks, ends, shallow surfaces, fused structures, and curved shallow surfaces, allowing for effective trapping and subsequent breakdown. Wang and colleagues<sup>117</sup> developed a Janus  $\text{Au@Ni@TiO}_2$  microrobot designed for microplastic removal. This microrobot utilizes an electrophoresis mechanism activated by UV light, allowing it to navigate through water. A model demonstrating the phoretic interaction between the  $\text{Au@Ni@TiO}_2$  micromotors and PS particles is shown in Fig. 3(c). The microrobot effectively captures microplastic particles from sources like personal-care products and Baltic seawater through this interaction. Additionally, these microrobots can form chains under the influence of an external magnetic field and move autonomously when exposed to UV light, facilitating the large-scale removal of MPs. The removal efficiency of the microrobot is

notable, achieving 77% in hydrogen peroxide ( $\text{H}_2\text{O}_2$ ) and 67% in pure water. Fig. 3(d) illustrates the movement tracks and speeds of the  $\text{Au@Ni@TiO}_2$  micromotor chains over a 2 s period in water under UV illumination.

Mayorga-Burrezo and colleagues<sup>118</sup> explored the use of light-powered catalysis combined with a transverse rotating magnetic field to drive  $\text{Fe}_3\text{O}_4@\text{BiVO}_4$  microrobots, examining the dynamics of their hybrid motion. When exposed to light, these microrobots generate reactive oxygen species (ROS), which, alongside magnetic propulsion, influence their movement. This dual stimulation can unexpectedly alter the microrobots' motion direction, as illustrated in Fig. 3(e). These hybrid-powered microrobots have been applied to tackle microplastic pollution, specifically targeting MPs found in cigarette filter residues, a significant source of environmental MPs. The study also investigated how varying concentrations of hydrogen peroxide ( $\text{H}_2\text{O}_2$ )

and different frequencies of the rotating magnetic field affect the hybrid motion. Time-lapse microscopy images showing the trajectories of individual  $\text{Fe}_3\text{O}_4/\text{BiVO}_4$  microrobots under these conditions are presented in Fig. 3(f) and (g). Martin's and Urso's team<sup>119</sup> recently developed an advanced multifunctional microrobot using MXene-derived  $\text{Fe}_2\text{O}_3/\text{Pt}/\text{TiO}_2$ , capable of capturing NPs in three-dimensional (3D) space under UV light (Fig. 4(a)). These microrobots demonstrated negative photogravitactic behavior when exposed to UV irradiation, enabling significant 2D and 3D motion (Fig. 4(b)). Numerical simulations showing the spatial distribution of hydrogen concentration over 0.1 s for two different configurations are illustrated in Fig. 4(c). The microrobots' surface charge, which can be adjusted through pH changes, greatly reduced the time needed for pre-concentration, leading to a dramatic increase in nanoplastic capture efficiency. Specifically, the microrobots achieved a 97% removal rate of 50-nm PS nanoparticles within just 1 minute, marking a significant enhancement over static MXene-based treatments (Fig. 4(d)). Beladi-Mousavi<sup>91</sup> developed an advanced photo-catalytic degradation system utilizing intelligent, visible-light-driven microrobots designed to capture and degrade MPs in complex multichannel environments. These microrobots are equipped with both photo-catalytic ( $\text{BiVO}_4$ ) and magnetic ( $\text{Fe}_3\text{O}_4$ ) materials, enabling self-propelled movement under sunlight and precise control *via* a

magnetic field within macrochannels. The microrobots, driven by visible light, effectively swim through aqueous media and adhere to various types of floating MPs, including polylactic acid (PLA), polycaprolactone (PCL), PET, and PP. They then degrade these plastics into smaller organic molecules and oligomers. The process of collecting different MPs using the photo-catalytic  $\text{BiVO}_4/\text{Fe}_3\text{O}_4$  microrobot in a macrochannel is demonstrated in Fig. 4(e), with the efficiency of microplastic collection shown in Fig. 4(f). Chattopadhy and colleagues<sup>120</sup> developed an effective method for removing MPs using self-asymmetric Pac-Man  $\text{TiO}_2$  microrobots. These microrobots not only collect MPs but also facilitate their photo-catalytic degradation. The hydrodynamic effects of the micromotors enhance their ability to attract and accumulate MPs in their vicinity. By combining self-propulsion, the phoretic assembly of passive colloids, and photo-catalytic oxidation, the team created a highly scalable and inherently asymmetric Pac-Man  $\text{TiO}_2$  micromotor. This microrobot is capable of actively capturing and degrading MPs, specifically homogeneous PS microspheres, to allow for precise optical degradation measurements.

The Pumera group<sup>121</sup> has conducted several studies on the use of photo-catalytic microrobots (MNRs) for the degradation of microplastic particles (MNPs). One notable development involves visible-light-driven microrobots based on  $\text{Bi}_2\text{WO}_6$

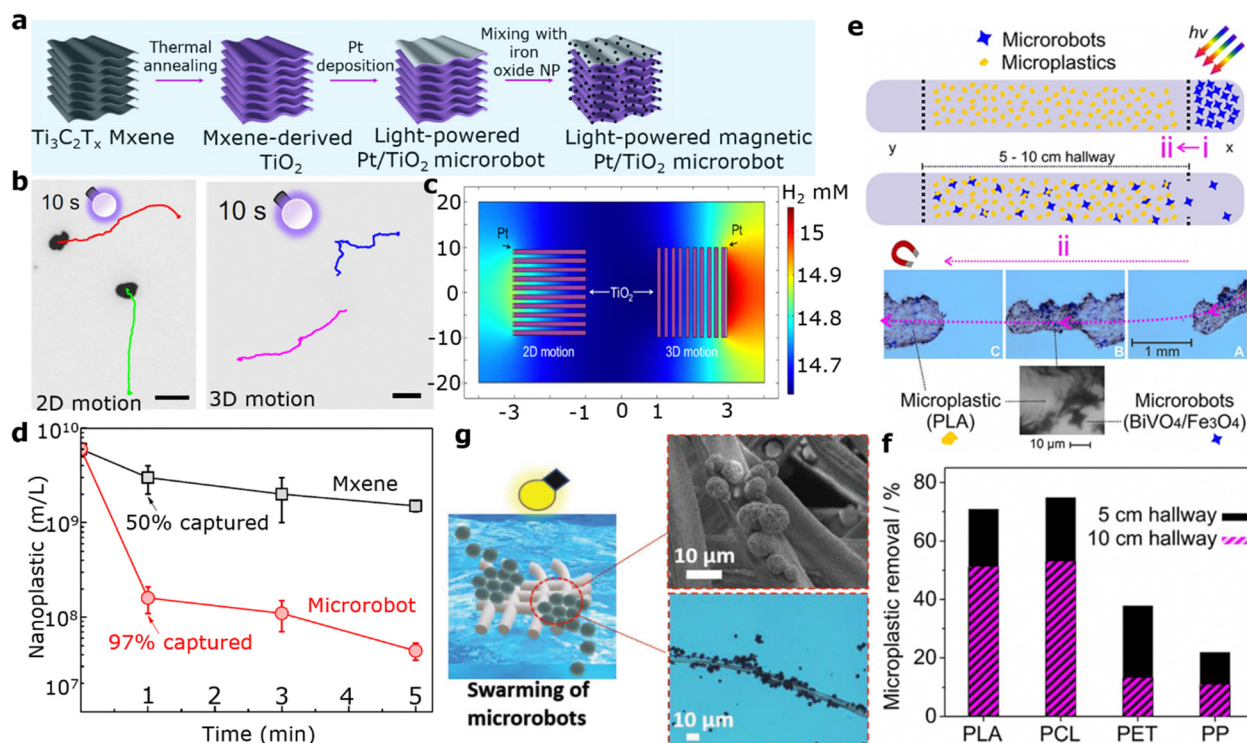


**Fig. 4** Scheme of the fabrication stages for  $\gamma\text{-Fe}_2\text{O}_3/\text{Pt}/\text{TiO}_2$  microrobots derived from MXene (a), movement of the microrobot in the xy plane (2D motion) and the xyz space (3D motion) (b), the spatial distribution of  $\text{H}_2$  concentration for the cross-section of the two configurations numerically simulated in 0.1 s (c) and nanoplastic capture (d). Adapted from ref. 119. Copyright 2022, Nature Portfolio. Schematic illustration of the extraction of MPs in an improvised channel *via*  $\text{BiVO}_4/\text{Fe}_3\text{O}_4$  microrobots; i → ii: illuminating of microrobots onto MPs; ii: adhesion of microrobots on a surface of MPs and transmission of a microplastic fragment decorated with microrobots (e), the efficacy of the accumulation of various MPs (f), and  $\text{Bi}_2\text{WO}_6$  microrobots swarming together when exposed to light and sticking to cloth strands (g). Adapted from ref. 91 and 121. Copyright 2011, the American Chemical Society and Copyright 2020, Wiley. The bars on the scale are 10  $\mu\text{m}$ .



designed to degrade textile fibers. As illustrated in Fig. 6(a), these microrobots can autonomously move under visible light, even at low fuel concentrations (0.025 wt %  $\text{H}_2\text{O}_2$ ). The microrobot swarms exhibit collective behavior and aggregate on the surface of textile fibers due to chemical gradients that induce permeation and electrophoretic interactions (Fig. 4(g)). Under UV light, the fiber network begins to collapse, with scanning electron microscopy revealing surface damage and pore formation of 0.3–0.6 mm in diameter, indicating partial degradation. This is due to the generation of reactive species, such as hydroxyl radicals, during photocatalysis, which attack the fiber surface and create pores, making it more vulnerable to further degradation.

Jancik-Prochazkova and colleagues<sup>122</sup> developed antimony sulfide-based microrobots decorated with magnetite nanoparticles for microplastic degradation. These microrobots utilize two independent propulsion modes: magnetic field and light irradiation. Due to their phoretic interactions, the microrobots show a preference for poly(3-hydroxybutyrate) (PHB) and poly(lactic acid) (PLA) MPs, facilitating their transport in a transverse rotating magnetic field (Fig. 5(a)). The photo-catalytic activity of  $\text{Sb}_2\text{S}_3$  quantum dots enables these microrobots to degrade MPs under UV light without additional fuel. For example, the molecular weight of PHB MPs decreased from 16 000 to 11 000  $\text{g mol}^{-1}$  after photodegradation, both with and without an external magnetic field. When the magnetic field is applied, the microrobots help push the MPs attached to their surface (Fig. 5(b)). The degradation of PHB and PLA by light-driven microrobots is demonstrated in Fig. 5(c) and (d). Additionally, Jancik-Prochazkova's team<sup>123</sup> introduced an innovative approach that involves engineering various point defects and incorporating platinum (Pt) single atoms onto titanium dioxide nanotubes, resulting in  $\text{TiO}_2\text{-NT}$ ,  $\text{TiO}_2\text{-HNT}$ , and  $\text{TiO}_2\text{-SA-NT}$  nanorobots (Fig. 5(e)). The  $\text{TiO}_2\text{-SA-NT}$  nanorobots displayed the highest negative photogravitaxis under UV light, while  $\text{TiO}_2\text{-HNT}$  nanorobots achieved the highest velocity in 2D. Both types of nanorobots showed a strong affinity for MPs and demonstrated the ability to irreversibly capture them. Fig. 5(f) and (g) illustrate the chemical gradient generated around  $\text{TiO}_2\text{-NT}$  nanorobots after UV irradiation and their “standup” motion under bottom illumination. Fig. 5(h) shows how light-induced self-orientation leads to the 3D motion of single  $\text{TiO}_2\text{-NT}$  nanorobots.

Guo and colleagues<sup>124</sup> reported a smart light-driven hydrogel actuator with a hierarchical structure, integrating covalently bonded polyethyleneimine and polydopamine copolymers, graphene oxide nanosheets, and poly(*N*-isopropylacrylamide) hydrogels (Fig. 5(i)). This actuator functions as an adsorbent for microplastic contaminants (MCPs), a photothermal converter, and an actuating matrix. The hierarchical design allows the actuator to perform as a soft swimming robot capable of identifying and adsorbing MCPs while maintaining high responsiveness. The hydrogel actuator exhibits an ultralow detection limit (0.98  $\mu\text{M}$  for ferric ions), excellent selectivity (97.09% for ferric ion-adsorbed MCPs), high adsorption (94.63%), and desorption efficiency (99.12%), alongside multiple photothermal actuation capabilities.

Moreover, light-powered robots have found diverse applications in real-world scenarios due to their ability to harness sustainable energy from light sources, typically solar energy.<sup>47</sup> In environmental monitoring, autonomous solar-powered robots are deployed to collect data on water quality, atmospheric conditions, and weather patterns. These robots operate continuously without the need for frequent recharging, making them ideal for remote and large-scale environmental studies. In the agricultural sector, light-powered robotic systems are utilized for precision farming tasks, including crop monitoring, irrigation management, and pesticide application, reducing reliance on conventional energy sources.<sup>125</sup> In healthcare, advancements in micro-robotics have led to the development of light-driven robots capable of performing targeted drug delivery and non-invasive diagnostic procedures by converting light energy into mechanical motion. Additionally, light-driven robotic systems are gaining traction in water purification and pollutant degradation due to their energy-efficient operation.<sup>19</sup>

One significant emerging application of light-powered robots is in microplastic removal. Photocatalytic robots equipped with materials such as titanium dioxide ( $\text{TiO}_2$ ) utilize solar energy to generate reactive species that can break down plastic contaminants in aquatic environments.<sup>14</sup> These systems offer a sustainable solution for mitigating plastic pollution by enabling the degradation or trapping of microplastics while consuming minimal external energy. The integration of autonomous navigation with light-driven propulsion allows these robots to cover vast water surfaces, improving the efficiency and scalability of cleanup operations. By leveraging renewable light energy and advanced catalytic systems, light-powered robots present a promising technology for addressing critical environmental challenges, including microplastic pollution.<sup>126</sup>

### 3.2. Magnet-powered robots for plastic removal

Magnetic microrobots offer considerable versatility and can be controlled through various external magnetic fields.<sup>127</sup> For example, a rotating magnetic field can induce rolling motion, while a gradient magnetic field can guide the microrobots in a straight path, either in a fixed posture or with a specific part of their structure maintained in place.<sup>128</sup> Combining these fields creates an alternating magnetic field, which drives the microrobots with asymmetric reciprocating motions.<sup>129</sup> This technology allows for precise, remote, and wireless manipulation and is applied across multiple domains, including biomedical therapy, swarm robotics, and environmental cleanup.<sup>130</sup>

Sun *et al.*<sup>131</sup> developed a “hedgehog” magnetic robot using sunflower pollen grains (SPGs) that excels in removing both oil and microplastic pollutants (Fig. 6(a)). Under a rotating magnetic field, the microrobot can switch between three motion modes: rolling, rotating, and swinging. In rolling mode, the microrobots can assemble into chains and transport 100- $\mu\text{m}$  PS microspheres (Fig. 6(b)). By combining rolling and swinging modes, these microrobots can efficiently capture, transport, and release MPs, achieving removal efficiencies of 75% and 70% in facial cleanser samples and contaminated seawater, respectively.

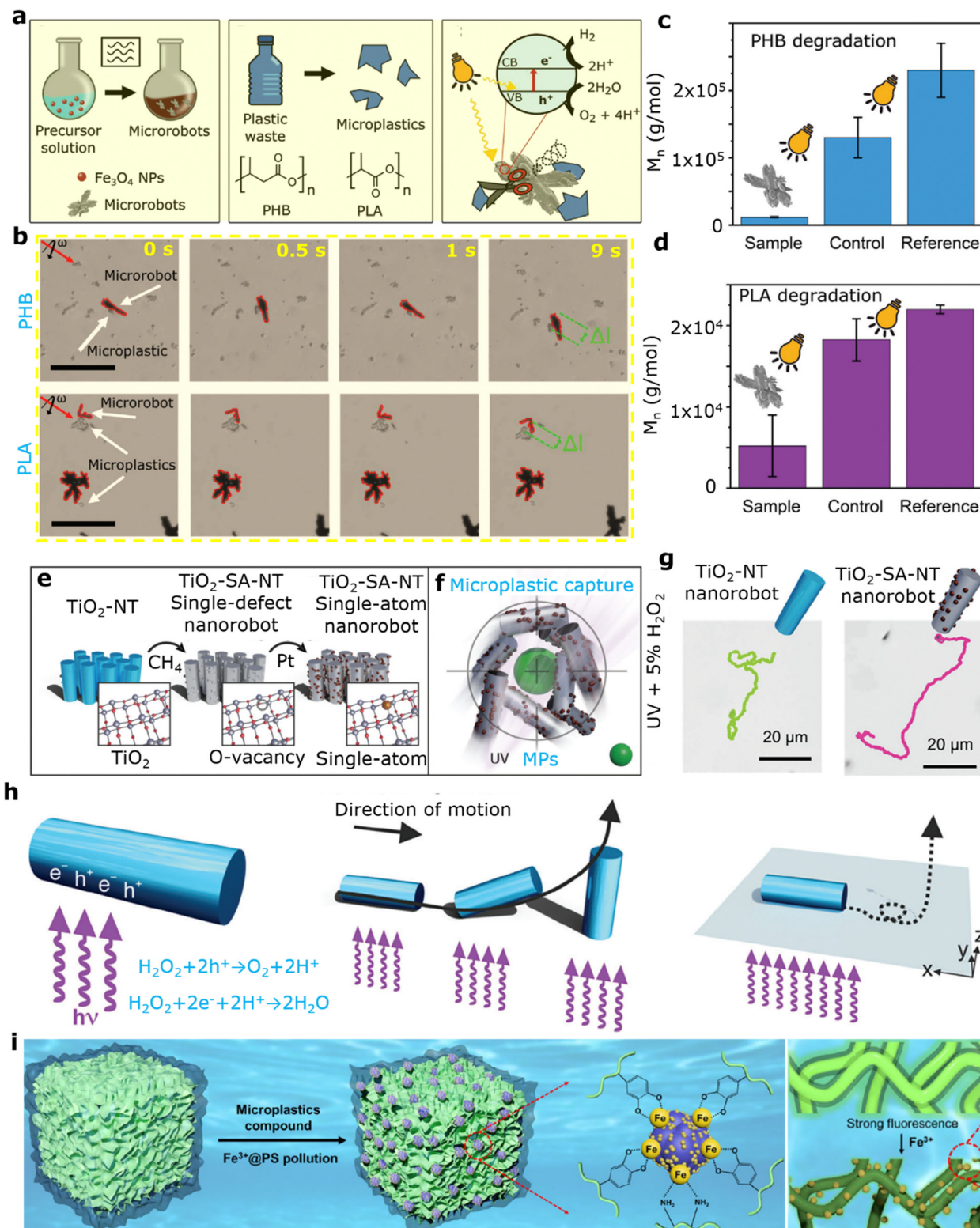


**Fig. 5** The photo-catalytic degradation of MPs during the breakdown process of plastic trash (a), microrobots are used to collect and move MPs, while the edges of PHB and PLA MPs are colored red (b), the scale bar is 50 μm. Using light-propelled microrobots to track PHB (c) and PLA (d). Adapted from ref. 122. Copyright 2023, Wiley-VCH. Formation of TiO<sub>2</sub>-HNT nanorobots and TiO<sub>2</sub>-SA-NT nanorobots (e), MPs are caught by them (f), a diagram showing the variation of chemical species produced by light and how they are rearranged (g), and light-driven self-orientation that makes a single TiO<sub>2</sub>-NT nanorobot move in three dimensions (h). Adapted from ref. 123. Copyright 2024, Springer. The hydrogel material with microplastic absorption (i). Adapted from ref. 124. Copyright 2022, the Royal Society of Chemistry.

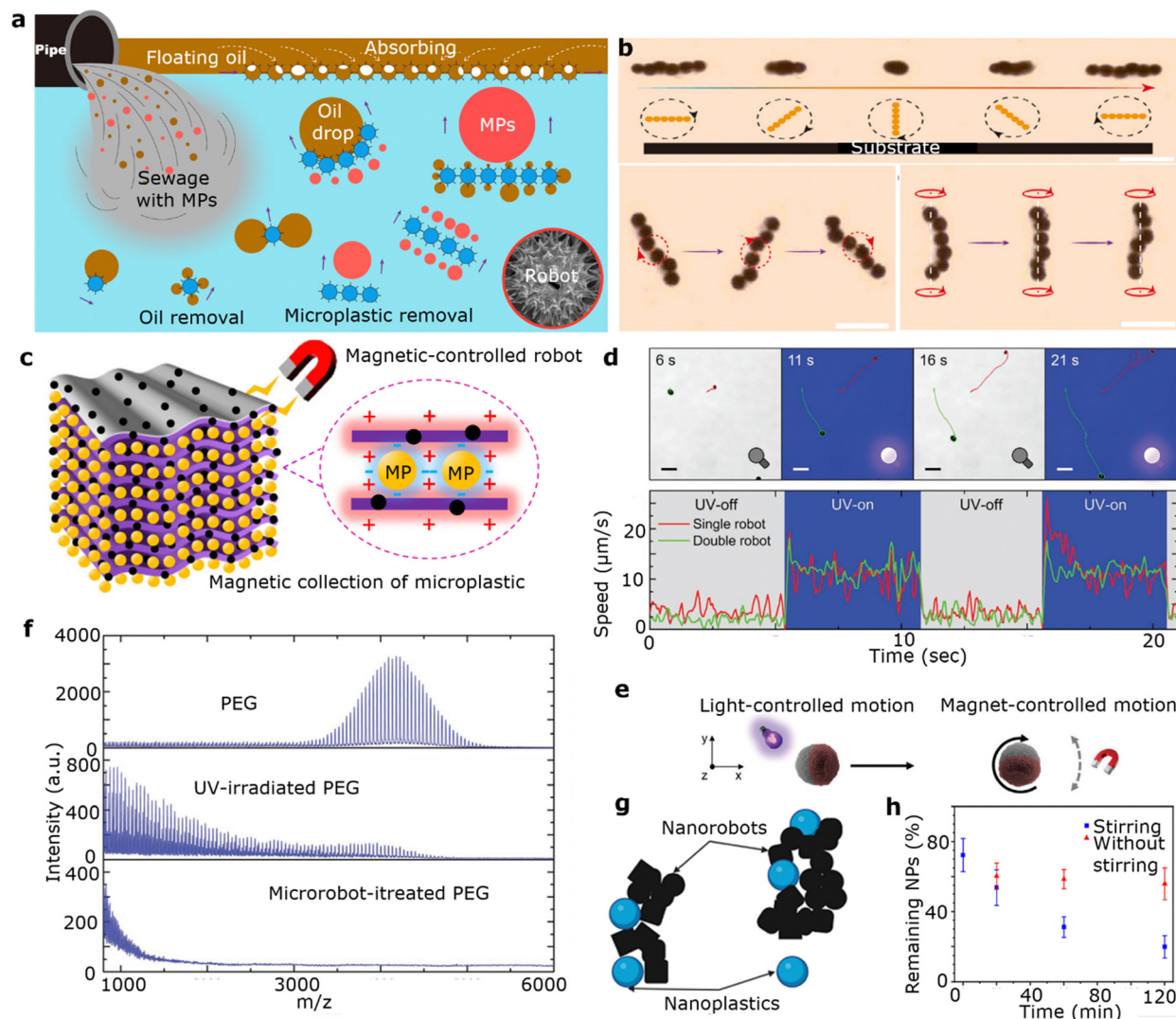


**Fig. 6** Strategy for using joint micros submarines to remove MPs (a) and putting together magnetic micros submarines on their own from different angles (b). Adapted from ref. 131. Copyright 2021, Elsevier. MPs were magnetically taken from the cleaned water using microrobots made from MXene-derived  $\text{Fe}_2\text{O}_3/\text{Pt}/\text{TiO}_2$  (c). Adapted from ref. 119. Copyright 2022, Springer. Images of single and double microrobots moving over time as UV light is turned on and off (scale bars are  $20\ \mu\text{m}$ ) (d), paths of a magnetic field-navigated microrobot that is controlled by light (e) and MALDI-MS profiles for the photodegradation of PEG (f). Adapted from ref. 132. Copyright 2021, Springer. A diagram of the cluster, with the nanorobots in black and the NPs in blue (g) and the amount of NPs that was left over after the different methods of removal (h). Adapted from ref. 133. Copyright 2024, the American Chemical Society.

Urlo *et al.*<sup>119</sup> reported on microrobots with a platinum (Pt) layer and magnetic  $\gamma\text{-Fe}_2\text{O}_3$  nanoparticles. These MXene-derived  $\text{Fe}_2\text{O}_3/\text{Pt}/\text{TiO}_2$  microrobots exhibit negative photogravitaxis and powerful fuel-free motion with six degrees of freedom when exposed to light. The microrobots use their unique self-propulsion and programmable zeta potential to quickly attract and trap NPs, including those in multi-layered structures, facilitating magnetic collection (Fig. 6(c)). These microrobots serve as self-motile preconcentration platforms for electrochemical detection of NPs with low-cost, portable electrodes. In a similar vein, Urlo *et al.*<sup>132</sup> also introduced self-propelled, light-powered, magnetic-field-navigable hematite/metal Janus microrobots (Fig. 6(d)–(f)).

Velikov *et al.*<sup>133</sup> presented a straightforward method for detecting and quantifying NPs in water using magnetic nanorobots

(Fig. 6(g)). NPs were stained with a hydrophobic fluorescent dye, allowing detection and quantification through photoluminescence techniques. The magnetic nanorobots captured and removed over 90% of NPs from an aqueous solution within 120 minutes (Fig. 6(h)). This approach demonstrates that common fluorescent dyes combined with photoluminescence spectroscopy can effectively detect and quantify NPs, with magnetic nanorobots facilitating their removal.

Urso *et al.*<sup>10</sup> also investigated biohybrid microrobots that integrate the magnetic properties of  $\text{Fe}_3\text{O}_4$  nanoparticles (Fig. 7(a)). These microrobots, which incorporate algae cells coated with  $\text{Fe}_3\text{O}_4$  nanoparticles, achieve precise locomotion and wireless manipulation through external magnetic fields. Magnetic algae robots (MARs) displayed significant efficiency in capturing and



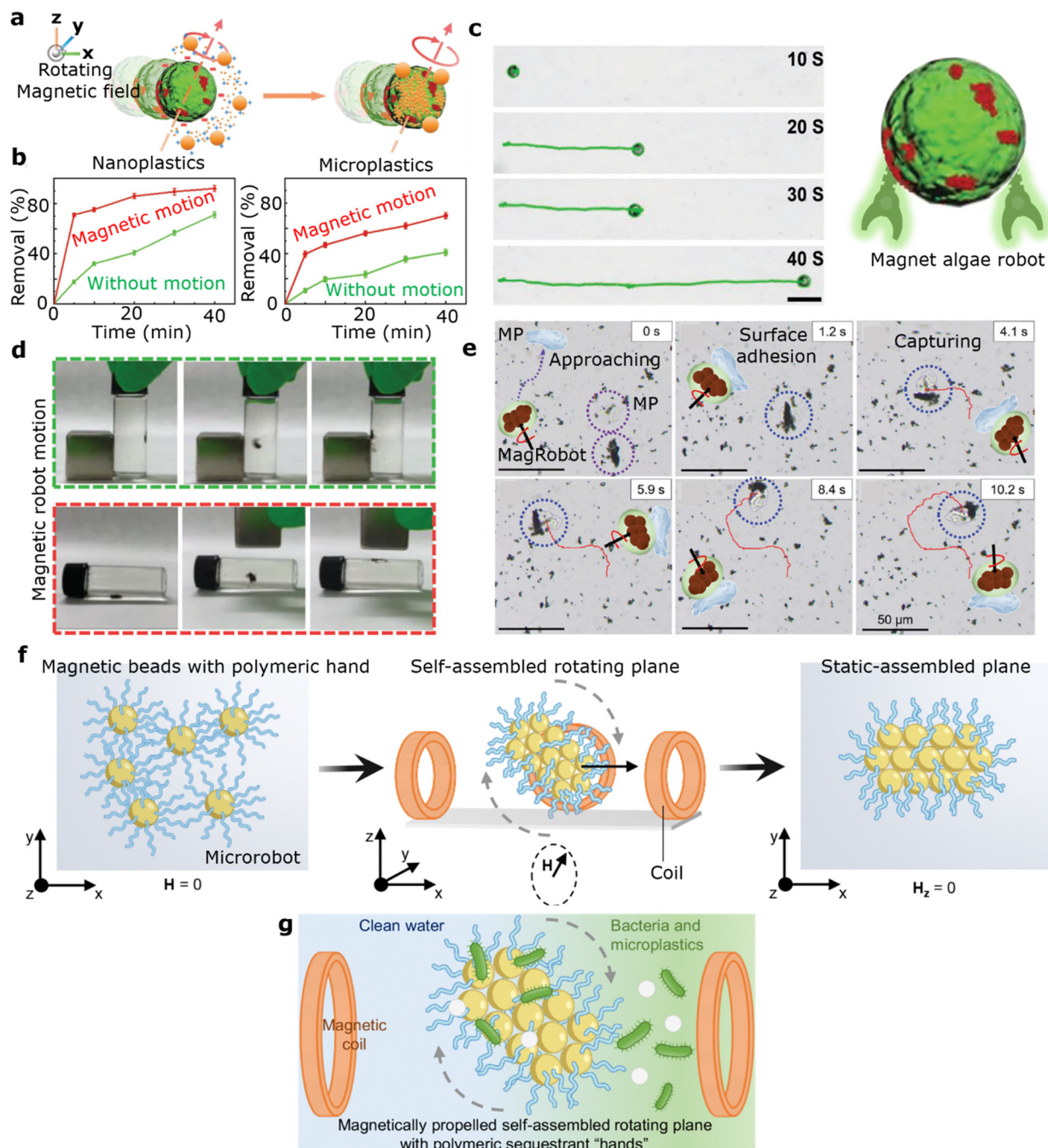


**Fig. 7** MARs move when there is a spinning magnetic field (a), MARs remove MNPs (b), time-lapse micrographs were made by turning the spinning magnetic field on and off (the scale bar was 10  $\mu$ m) (c) and using a fixed magnet to change the magnetic property of MARs will allow exact handling by using an outside magnetic field (d). Adapted from ref. 10. Copyright 2024, Springer. Microplastic removal process using PDA@Fe<sub>3</sub>O<sub>4</sub> MagRobots (e). Adapted from ref. 134. Copyright 2021, John Wiley & Sons. The movement of groups of microrobotic planes over time (f), and magnetic microrobots made of polymers that can pick up bacteria and MPs (g). Adapted from ref. 126. Copyright 2024, the American Chemical Society.

removing MNPs from water, with extensive potential applications (Fig. 7(b)). Time-lapse micrographs showing MARs in action with on/off switching of the rotating magnetic field are depicted in Fig. 7(c). The reusability of MARs was also assessed, demonstrating excellent recyclability. The permanent magnet used for MARs ensures precise control *via* external magnetic fields (Fig. 7(d)).

Zhou *et al.*<sup>134</sup> developed innovative adhesive polydopamine (PDA)@Fe<sub>3</sub>O<sub>4</sub> magnetic microrobots (MagRobots), inspired by the adhesive properties of marine mussels. These MagRobots are created by coating Fe<sub>3</sub>O<sub>4</sub> nanoparticles with a dopamine-based polymer through a single-step self-polymerization process. To enhance their functionality, lipase enzymes are incorporated onto the surface of the PDA@Fe<sub>3</sub>O<sub>4</sub> MagRobots,

enabling them to degrade MPs enzymatically. These synthesized MagRobots are controlled externally using a rotating magnetic field, which allows them to effectively target and remove MPs due to their strong adhesive properties (Fig. 7(e)). The MPs, once bound to the MagRobots, can be guided along a predetermined path and removed using directional magnetic fields.

Furthermore, Ussia *et al.*<sup>126</sup> introduced a different type of magnetically controlled microrobot, characterized by polymeric “hands” surrounding a magnetic core. These microrobots, as shown in time-lapse images, self-assemble into organized, rotating planes of varying sizes under external magnetic field influence (Fig. 7(f) and (g)). This self-assembly enables them to adjust their propulsion speed and exhibit coordinated movement, allowing them to actively capture both free-swimming bacteria and dispersed MPs. Unlike traditional methods, these

microrobots can be efficiently retrieved from complex environments and can release the captured contaminants into another vessel in a controlled manner using ultrasound, providing a sustainable approach for repeated decontamination. Additionally, UV irradiation of the remaining water ensures the elimination of any residual bacteria, offering a thorough cleaning solution.

Zhang *et al.*<sup>135</sup> developed keratin (KER)-based biohybrid micro/nanorobots (KMNRs) by decorating iron-oxide microspheres with magnetic properties (Fig. 8(a)). These KMNRs are engineered to effectively remove MPs and NPs through a combination of chemical and physical interactions, precise magnetic control, and enhanced surface functionalities. The integration of iron-oxide microspheres allows these biohybrids to be accurately moved and manipulated using an external magnetic field. The relationship between the speed of the KMNRs and magnetic field intensity at a

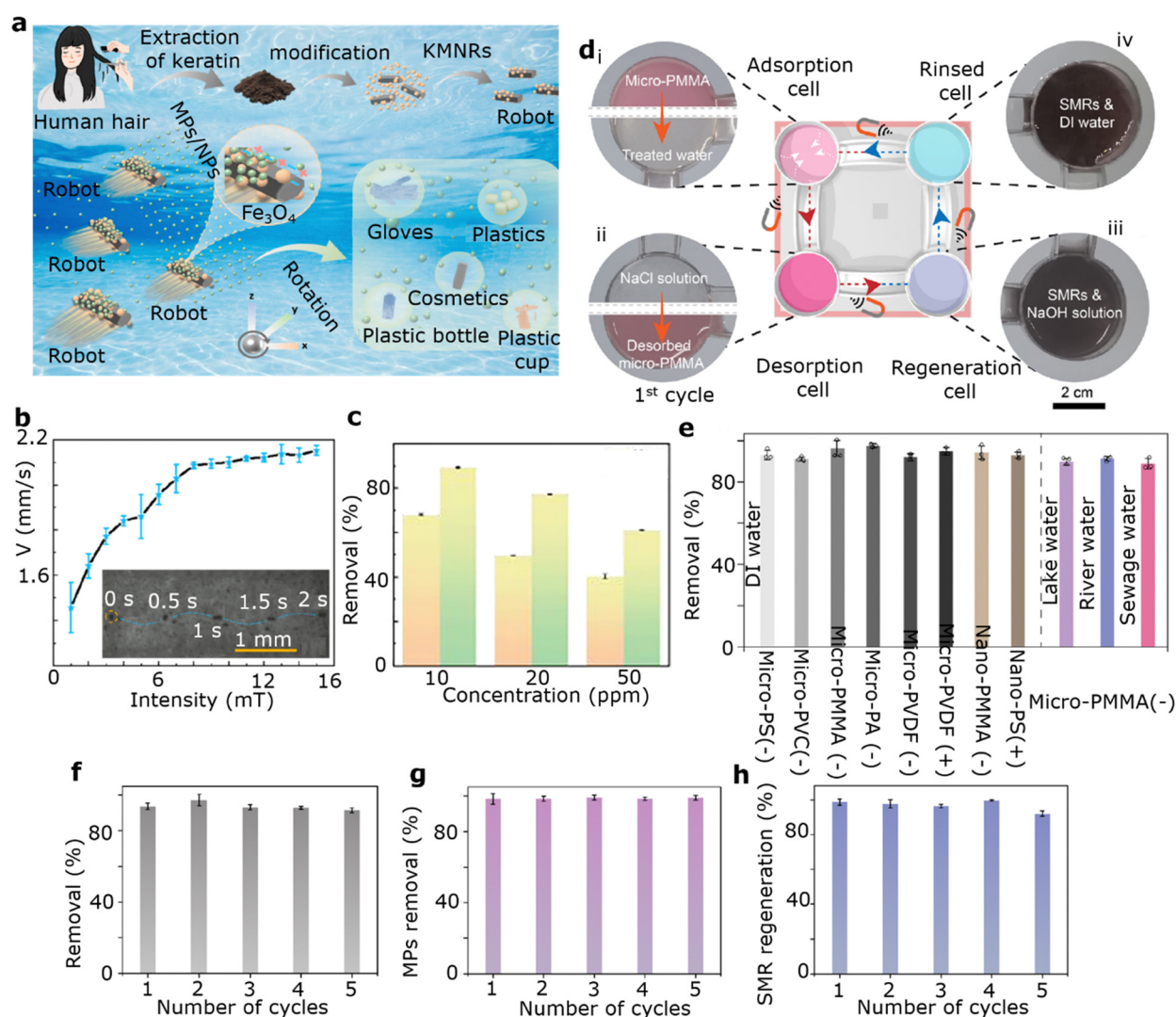


**Fig. 8** A schematic of removing keratin fibers from human hair and the lower part on the right shows the form of KMNRs and the role they play in absorbing MPs/NPs (a). KMNRs' speed and strength are related, and a time-lapse of KMNRs is shown in the bottom left corner (b) and a graph representing the removal of MPs is given (c). Adapted from ref. 135. Copyright 2024, Elsevier. There are four linked cells for cycling MNP elimination, MNP desorption, SMR regeneration, and SMR rinsing (d). The removal rates for MNPs in different media (e), removal efficiency (f), MP desorption rates (g), and SMR regenerating rates (h) over five cycles. Adapted from ref. 136. Copyright 2022, the American Association for the Advancement of Science.

fixed frequency of 6 Hz is illustrated in Fig. 8(b). These fuel-free keratin magnetic micro/nanorobots demonstrated high removal efficiencies in water, achieving 95% for MPs and 82% for NPs (Fig. 8(c)).

Li *et al.*<sup>136</sup> introduced a self-propelled magnetorobot made from a magnetizable ion-exchange resin sphere, designed to effectively remove or separate MNPs from various nonmarine water sources (Fig. 8(d)). The removal efficiency of MNPs in different water types, including deionized, river, lake, and sewage water, is shown in Fig. 8(e). Thanks to the long-range electrophoretic attraction generated by the recyclable ion-exchange resin, this magnetorobot demonstrated a consistent MNP removal efficiency of over 90% across five treatment cycles. Additionally, it proved to be broadly applicable, successfully handling different plastic types, sizes, shapes, and various nonmarine water samples (Fig. 8(f)–(h)).

### 3.3. Fuel-powered robots for plastic removal

Fuel-driven micro- and nanorobots, often referred to as ‘chemical’ or ‘catalytic’ robots, utilize the interaction between a catalyst and a chemical fuel to generate movement.<sup>137</sup> Chemical-driven robots often rely on catalytic and fuel systems to generate propulsion and energy for movement. One widely used fuel is hydrogen peroxide ( $\text{H}_2\text{O}_2$ ), which is environmentally friendly and highly reactive. When decomposed by catalysts such as platinum (Pt), manganese dioxide ( $\text{MnO}_2$ ), or iron oxide ( $\text{Fe}_3\text{O}_4$ ),  $\text{H}_2\text{O}_2$  breaks down into water ( $\text{H}_2\text{O}$ ) and oxygen gas ( $\text{O}_2$ ), releasing heat and producing bubbles that generate thrust for locomotion.<sup>138</sup> The efficiency of this catalytic decomposition depends on factors such as the concentration of  $\text{H}_2\text{O}_2$ , catalyst type, and surface area. Catalysts with a higher surface area typically facilitate faster decomposition, leading to better propulsion performance.<sup>139</sup> However, high-salinity environments pose significant challenges to these systems. Salt ions, particularly sodium and chloride ions, can adsorb onto catalyst surfaces, reducing their efficiency by blocking active sites. Additionally, salt-induced electrochemical corrosion compromises the durability of catalytic components. The increased viscosity and surface tension of saline water further hinder bubble formation and release, reducing thrust efficiency.<sup>140</sup>

To overcome these challenges, several strategies have been developed. Protective coatings made from corrosion-resistant materials, such as graphene, silica, or polymers, help shield catalysts from salt corrosion while maintaining catalytic efficiency. Nanostructured catalysts with enhanced surface area and engineered properties offer improved performance in saline environments. Hybrid catalytic systems that combine multiple catalysts can also provide greater stability and efficiency. Modifying the hydrophobicity of catalyst surfaces enhances bubble release, improving thrust generation.<sup>141</sup> Additionally, stabilizing  $\text{H}_2\text{O}_2$  formulations or blending it with other fuels helps maintain consistent propulsion in saline conditions. These advancements enable chemical-driven robots to perform effectively in high-salinity environments, making them suitable for applications such as oceanographic research, environmental monitoring, and marine exploration. The ability of these

robots to autonomously generate thrust without external power sources makes them invaluable for operations in remote and harsh marine environments.<sup>142</sup>

The reaction powers the robots through mechanisms like bubble propulsion or self-phoresis, which is the autonomous movement of a particle in response to a gradient, such as concentration (self-diffusiophoresis), electric potential (self-electrophoresis), or temperature (self-thermophoresis).<sup>143</sup> For example, Pt microrockets are propelled in  $\text{H}_2\text{O}_2$  by the continuous release of oxygen ( $\text{O}_2$ ) bubbles (Fig. 9(a)), providing strong thrust and enabling movement even in high-ionic-strength environments like seawater. Biological enzymes like catalase, urease, and glucose oxidase act as natural counterparts to inorganic catalysts. Micro- and nanorobots with an uneven distribution of catalase, which breaks down  $\text{H}_2\text{O}_2$ , can move *via* bubble propulsion, while robots using urease and glucose oxidase catalyze reactions with more biocompatible substrates like urea and glucose, creating gradients that drive self-phoresis (Fig. 9(b)).<sup>19</sup> However, the application of these enzymes is mostly limited to biomedical contexts where these substrates naturally occur, such as in the bladder for urea.<sup>144,145</sup> Additionally, the robots can disintegrate through catalytic reactions that consume both the robot’s engine and fuel, similar to how magnesium reacts with water (Fig. 9(c)). Despite their potential, these fuel-driven robots often suffer from limited control over their movement (*e.g.*, on-off switching and directionality) and have a short operational lifespan.<sup>143,146</sup>

Catalytic microrobots made from manganese dioxide ( $\text{MnO}_2$ ) have also been used to efficiently remove various organic pollutants, propelled by bubbles generated from  $\text{H}_2\text{O}_2$  decomposition.<sup>148</sup> Adsorptive bubble separation (ABS) is a technique widely employed to separate solid particles, droplets, or other suspended matter from liquids.  $\text{MnO}_2$ -based microrobots, which produce numerous bubbles during  $\text{H}_2\text{O}_2$  decomposition, offer a promising method for pollutant removal through this bubble separation mechanism.<sup>149</sup>

In a recent study, Ye *et al.*<sup>147</sup> designed magnetic microrobots with a core-shell structure composed of  $\text{Fe}_3\text{O}_4$ - $\text{MnO}_2$  and  $\text{Fe}_2\text{O}_3$ - $\text{MnO}_2$  using scalable hydrothermal methods (Fig. 9(d)). These microrobots effectively removed MPs through the ABS mechanism using a 5% concentration of  $\text{H}_2\text{O}_2$ . As the microrobots moved, they trapped MPs in the microbubbles formed by  $\text{H}_2\text{O}_2$  decomposition, which then accumulated on the surface foam layer, making them easy to separate (Fig. 9(e)). Photographs showing the progress of microplastic removal over 1 to 6 hours are presented in Fig. 9(f). This ABS method achieved a microplastic removal efficiency of 10% after a 2-hour treatment.

### 3.4. Ion-exchange-powered robots for plastic removal

Ion-exchange-based microrobots (MNRs) have gained significant attention due to their ability to self-assemble and exhibit swarming behavior.<sup>136</sup> Urlo *et al.*<sup>132</sup> reported self-propelled hematite/metal Janus microrobots. These Janus microrobots, created by asymmetrically depositing metals onto hematite microspheres, exhibit higher speeds with bimetallic coatings compared to single metals (Fig. 6(d)). This enhancement is due



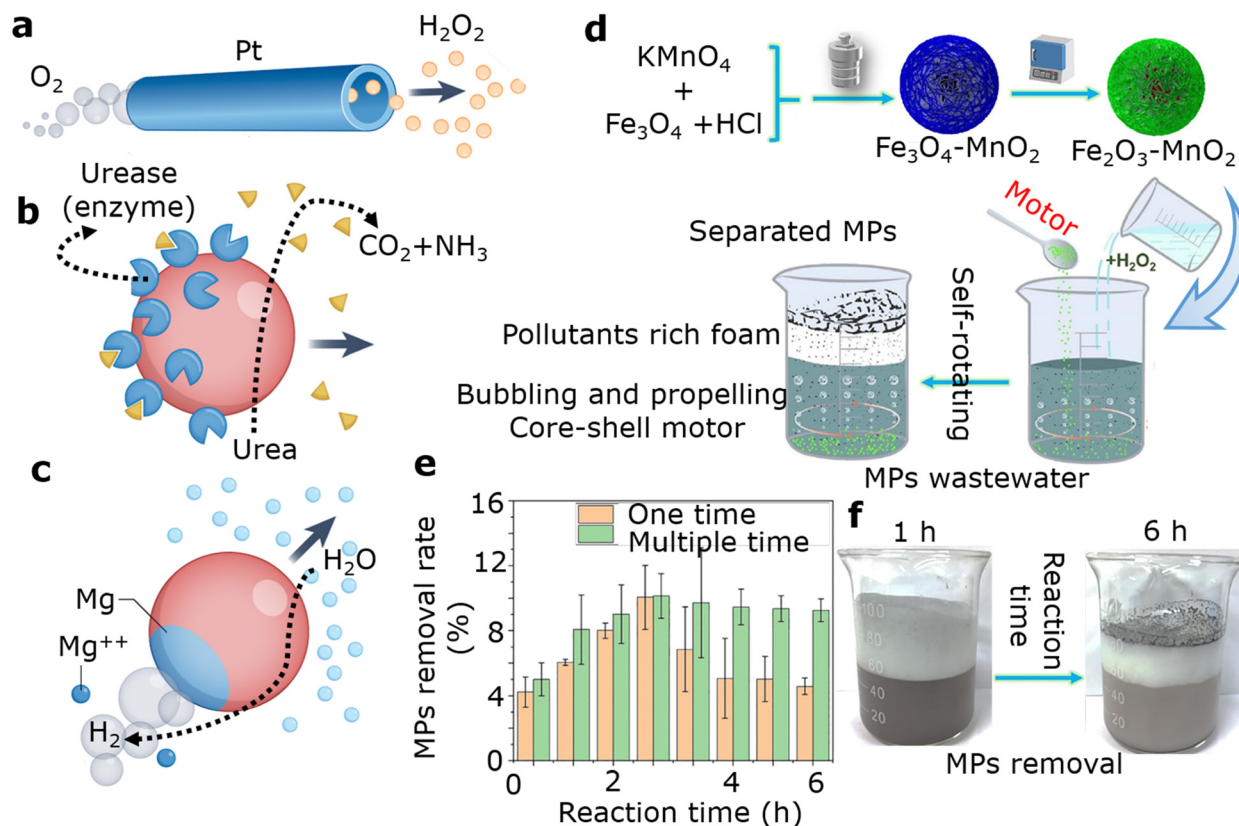
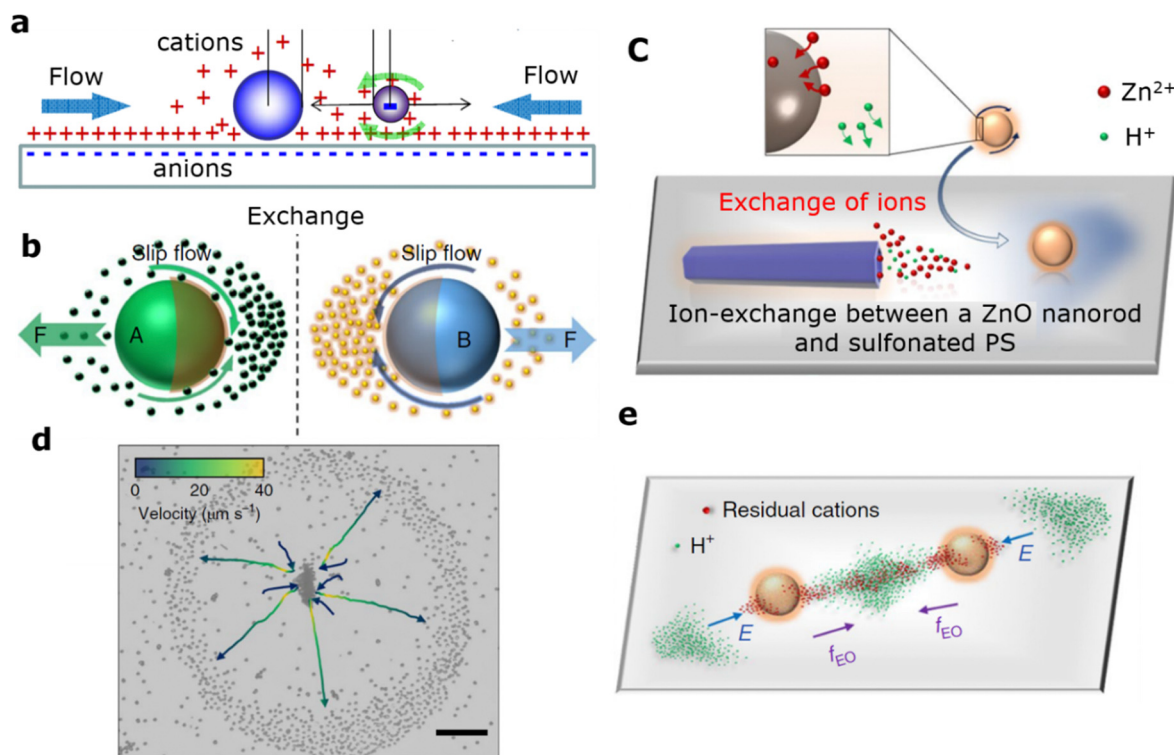


Fig. 9 Pt microrobot movement and  $\text{H}_2\text{O}_2$  is broken down into  $\text{O}_2$  bubbles (a), nanorobots driven by enzymes to break down urea (b) and microrobots based on magnesium to make  $\text{H}_2$  bubbles (c). Adapted from ref. 19. Copyright 2023, Springer Nature. Making core-shell magnetic micromotors and adsorptive bubble separations for eliminating of MPs and liquid pollutants (d), the way MPs get rid of things (e) and views of the reaction beakers used to get rid of MPs after 1 to 6 hours of reaction time (f). Adapted from ref. 147. Copyright 2021, Elsevier.

to improved microrobot motion, better electrostatic capture of polymer chains, enhanced charge separation at the hematite/metal interface, and a catalyzed photo-Fenton reaction (Fig. 6(e)). The MALDI-MS spectra shown in Fig. 6(f) reveal that UV exposure decreases the mass of PEG macromolecular chains, leading to the formation of oxidized polymer chains at lower masses.

Niu *et al.*<sup>150</sup> investigated a set of modular swimming microrobots that rely on cation exchange resins. Interestingly, while the resin particles themselves do not move on their own, they can self-assemble into active, propelling structures when mixed with inert particles (Fig. 10(a)). The resin particles exchange ions with impurities in the solution, and the exchanged cations and protons diffuse at different rates, creating a local diffusion electric field directed inward.<sup>151</sup> This electric field generates an electro-osmotic flow around the negatively charged substrate, which attracts inert particles toward the cation exchange resin. However, without the presence of inert particles, the fluid flow around the resin particles remains uniform and fails to generate directional movement. In contrast, when inert particles are asymmetrically adsorbed onto the resin, they disrupt the uniform flow, resulting in the autonomous movement of the resin particles. Therefore, the propulsion of ion-exchange MNRs is powered by the energy released during the ion exchange process, aided by the formation of an asymmetric structure.<sup>152</sup>

Moreover, Tang's and Wu's research groups<sup>153</sup> utilized ion-exchange reactions to create an active interaction system involving zinc oxide (ZnO) nanorods and sulfonated polystyrene (SPS) microbeads. As illustrated in Fig. 10(b), two chemically powered particles, A and B, each release chemical byproducts as they move. When mixed together, particles A and B engage in an exchange of these byproducts and nutrients, leading to enhanced reactivity and movement for both the ZnO nanorods and SPS microbeads. This chemical communication, driven by ion exchange, results in the formation of active swarming complexes. These complexes demonstrate behaviors such as phase segregation and collective decision-making, observable from microscopic to macroscopic scales. The ion-exchange mechanism proves to be a versatile approach for creating complex interactions between active and passive particles, paving the way for the development of responsive active materials and systems. Fig. 10(c) and (d) depict the formation of ZnO-sulfonated PS complexes, where sulfonated PS trajectories are color-coded based on their speeds. The overlapping gradients of residual cations and released  $\text{H}^+$  ions create an asymmetric electric field and subsequent electroosmotic flow, which facilitate the assembly of sulfonated PS particles (Fig. 10(e)). For applications involving the removal of MNPs using MNRs, it is essential to minimize energy input. Ideally, the use of



**Fig. 10** Different rates at which protons and swapped cations move (a). Adapted from ref. 150. Copyright 2017, the Royal Society of Chemistry. The way that different types of microswimmers (b), ZnO and sulfonated PS interact with electricity (c), ZnO–sulfonated PS complex forms with a ZnO nanorod (d) and protons interact with sulfonated PS electricity (e). Adapted from ref. 153. Copyright 2021, Nature Portfolio.

chemical fuels and external control devices should be avoided. The ion-exchange-driven mechanism offers an advantage in this regard, as it harnesses energy from the ion-exchange process itself, converting it into propulsion force without the need for additional fuels or complex external controls. This feature makes the ion-exchange mechanism particularly advantageous for large-scale, cost-effective applications.

Li *et al.*<sup>136</sup> developed a self-driven magnetorobot (SMR) that employs an ion-exchange mechanism to efficiently remove MNPs from non-marine waters in a scalable and reusable manner. The SMR is constructed from ion-exchange resin microspheres, which are functionalized with  $\text{Fe}_3\text{O}_4$  nanoparticles. This magnetic property allows for easy collection and separation, enabling cyclic operation and precise, magnetically-controlled adsorption. The effectiveness of SMRs in MNP removal, magnetic separation, and controlled release has been demonstrated, showcasing their versatility as a scalable solution. The SMRs achieve autonomous movement through the non-uniform adsorption of MNPs, which generates an asymmetric flow field that propels the robots. It was observed that the speed of the initial motion increased with the degree of asymmetry caused by adsorption. Importantly, SMRs do not require a pre-designed asymmetric structure, reducing both the complexity and cost of preparation. The propulsion efficiency and attraction range of SMRs are influenced by the ion-exchange capacity and the diffusion rate of the exchanged ions, with high-diffusivity ions like  $\text{H}^+$  and  $\text{OH}^-$  proving particularly

effective in enhancing SMR performance. A notable example is the OH-SMR, an anion-exchange resin-based SMR operating in a strong-base state with  $\text{OH}^-$  as the rechargeable ion. The OH-SMR captures impurity anions from the surrounding water and releases  $\text{OH}^-$ , creating a long-range pH gradient and a 3D adsorption field extending over 100 mm, effectively attracting negatively charged MNPs and significantly boosting removal efficiency. The SMRs have shown exceptional removal efficiencies, exceeding 90%, for MNPs of various compositions, sizes, and shapes in different non-marine water samples. To test their practicality, SMR removal efficiencies were compared with traditional methods at low MNP concentrations (10 and 20 ppm), which are about 10 times lower than typical environmental levels. SMRs outperformed traditional filtration and coagulation methods, achieving over 90% removal efficiency. Additionally, the SMRs maintained their performance over 100 treatment cycles, highlighting their excellent cycling stability and long-term recyclability. To further demonstrate the scalability of SMRs, a closed-loop miniplant for large-scale decontamination of MNP-contaminated water was established. The miniplant consisted of four units: MNP adsorption by SMRs, MNP desorption, SMR regeneration, and SMR rinsing with deionized water. The SMRs effectively removed colored MNPs from the water. After five consecutive cycles, a visible color change in the desorption cells confirmed the successful transfer of MNPs from the treated water. In this system, the removal efficiency, SMR regeneration rate, and MNP desorption rate all

exceeded 90%. This SMR-based dynamic adsorption technology offers several advantages, including simplicity, low cost, no need for chemical fuels, and suitability for industrial-scale applications. It presents a promising approach for MNP removal and separation across various settings.<sup>14</sup> However, the high ionic strength of seawater remains a challenge, and further improvements in salt resistance are necessary to expand the application of ion-exchange-based MNRs. Despite this, the technology represents a significant advancement in addressing MNP pollution, with ongoing developments needed to optimize its effectiveness in real-world environments.

### 3.5. Other multifarious-powered systems for plastic removal

Researchers have also investigated the use of light-thermal-driven micro- and nanorobots (MNRs) for removing MNPs.<sup>154</sup> These MNRs incorporate photothermal materials into Janus structures, enabling movement through temperature gradients generated by the photothermal effect. For example,<sup>155</sup> a sulfonated graphene gradient nanostructure-based MNR that utilizes light-thermal propulsion for microplastic removal. This microrobot is composed of a polyurethane (PU) matrix functionalized with  $\beta$ -cyclodextrin ( $\beta$ -CD)-modified sulfonated graphene (SG). The inclusion of  $\beta$ -CD in the PU matrix, facilitated by

hydrogen-bonding interactions, creates a gradient nanostructure that balances rigidity, enhances mechanical properties, and improves the material's usability and durability—qualities that are particularly advantageous for applications in soft robotics.<sup>156</sup> When exposed to near-infrared (NIR) light, the soft robot demonstrates rapid actuation, multiple actuation modes, and the ability to move in any direction. The bending and straightening motions of the microrobot are driven by the significant difference in thermal expansion coefficients between PU and SG, which leads to a mismatch in volume change between the two sides of the film. This deformation occurs at the specific location where NIR light is applied to the fish-shaped PU/ $\beta$ -CD-SG microrobot, and periodic alternation of NIR light causes the robot to perform a back-and-forth motion. Furthermore, the PU/ $\beta$ -CD-SG microrobot has shown excellent adsorption capabilities for MPs. Although initially smooth and flat, the surface of the microrobot becomes textured and lumpy after adsorbing MPs, and it can be reused up to 10 times, demonstrating its potential for sustainable microplastic removal.

Ho *et al.*<sup>157</sup> developed innovative and eco-friendly asymmetrically structured micromotors using a microfluidic technique, with the specific aim of efficiently removing large quantities of plastics from the environment.<sup>158</sup> These micromotors are

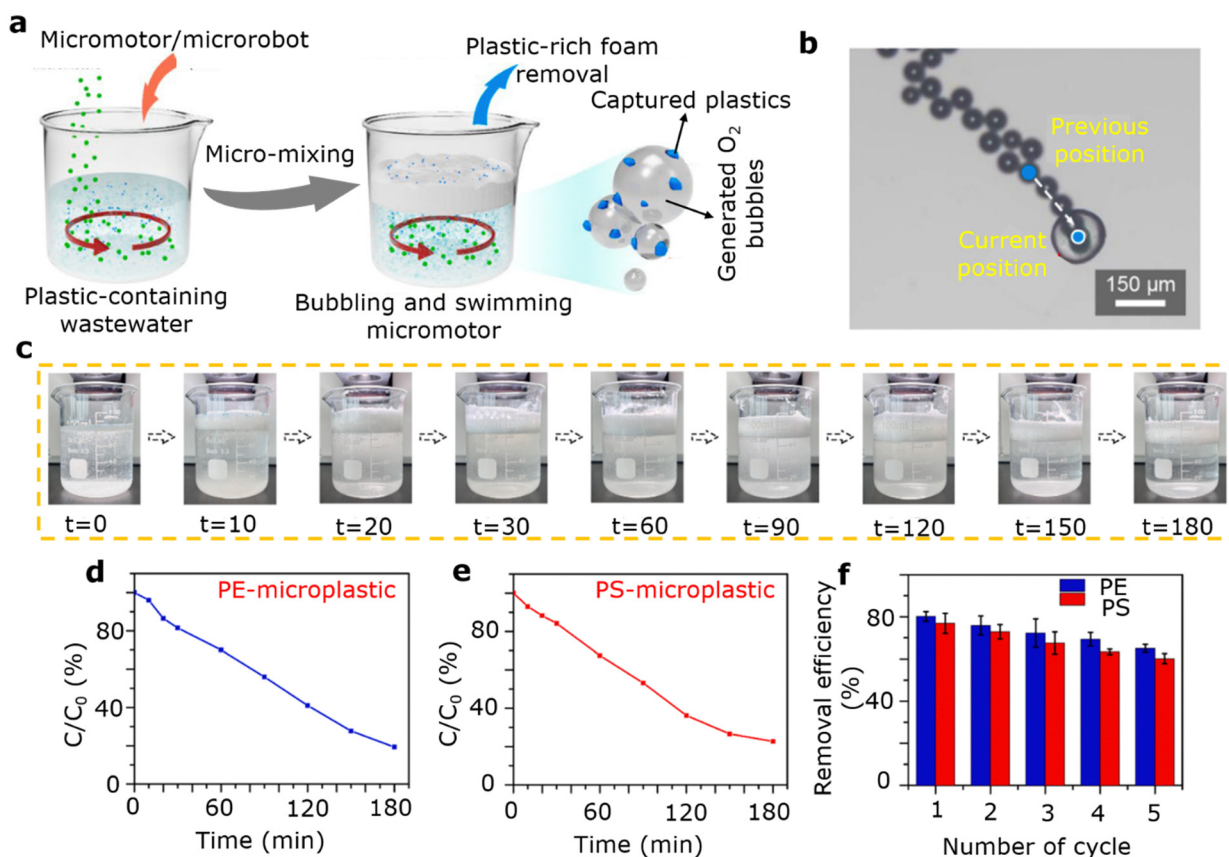


**Fig. 11** GO<sub>x</sub>/Cat micromotors can catch metals that are free to flow (a), the micromotor swimming on its own and the white dotted lines show the micromotor's path from its current place to a previous one (b), using GO<sub>x</sub>/Cat PEGDA micromotors for removal of MPs (c), the speed at which PEGDA micromotors bubbles (d, e) remove plastics and the ability of micromotor to remove MPs for five cycles (f). Adapted from ref. 157. Copyright 2024, Elsevier.



constructed from a polyethylene glycol diacrylate (PEGDA) matrix embedded with glucose oxidase ( $\text{GO}_x$ ) and catalase (Cat), as shown in Fig. 11(a). The microfluidic process allowed for the creation of micromotors with uniform yet asymmetric shapes through a combination of aqueous two-phase separation and UV polymerization. Additionally, the micromotors can be tailored with functional nanomaterials to meet specific wastewater treatment requirements.<sup>159</sup> The micromotors operate by utilizing  $\text{GO}_x$  and Cat to consume glucose as fuel, which in turn generates oxygen microbubbles. Upon introduction into a prepared wastewater solution, the micromotors rapidly start producing these bubbles.<sup>160</sup> The bubbles not only propel the micromotors but also capture suspended plastic nano- and

micro-particles, effectively extracting them from aquatic environments (Fig. 11(c)). The high surface tension of the bubbles facilitates the entrapment of plastics at the bubble interface, enabling their efficient removal from the water. The micromotors achieved notable removal efficiencies of 80.7% for MPs and 77.3% for NPs, as detailed in Fig. 11(d) and (e). A comprehensive reusability analysis was conducted by using the micromotors for five consecutive cycles of removing both polyethylene (PE) MPs and PS nanoplastics without any intermediate treatment, as illustrated in Fig. 11(f).

In parallel, Wang *et al.*<sup>161</sup> introduced an advanced technology, artificial intelligence-assisted nanodigital in-line holographic microscopy (AI-assisted nano-DIHM), capable of automatically

Table 1 Different kinds of robots for plastic removal

Robot	Motion controlled nature	Speed	Type of plastic	Size	Removal efficiency	No. of recycle	Mechanisms	Ref.
Au@Ni@TiO <sub>2</sub> -based micromotor	UV light	65.52	PS, PE	1–10 $\mu\text{m}$	67–77	—	Phoretic interactions and shoveling	117
SPG-based micromotors	Magnetic	104	PS	100 $\mu\text{m}$	70–75	6	Non-contact shoveling	131
Single-component TiO <sub>2</sub>	UV light	20	PS, PEG	500 nm	—	—	Photo-trapping and photo-fragmenting	116
MXene-derived Y-Fe <sub>2</sub> O <sub>3</sub> /Pt/TiO <sub>2</sub>	Magnetic	16	NPs	50 nm	66.7	4	Electrostatic interactions	119
Lipase-PDA-Fe <sub>3</sub> O <sub>4</sub>	Magnetic	4–6	PCL	20–50 $\mu\text{m}$	—	—	Chemical adhesion and enzymatic	134
Fe <sub>3</sub> O <sub>4</sub> -MnO <sub>2</sub> core-shell micromotors	Bubble propulsion	50–195	PE	25–30 $\mu\text{m}$	10	—	Adsorptive bubble separation	147
Pt-Pd-Fe <sub>2</sub> O <sub>3</sub>	UV light and magnetic	12	PEG	1–10 $\mu\text{m}$	—	—	Electrostatic interactions	132
Biomimetic robots	—	212 000	PS	850 $\mu\text{m}$	—	—	Vortex interactions	167
Fe <sub>3</sub> O <sub>4</sub> @BiVO <sub>4</sub>	Visible light and magnetic	5–10	PLA, PCL, PET, PP	100–200 $\mu\text{m}$	10–70	—	Adsorption and precipitation	91
Au-WO <sub>3</sub> @C Janus Micromotors	UV light	16	DCIP	—	80–85	5	Diffusiophoretic effect	112
Pac-Man TiO <sub>2</sub>	UV light	35–40	PS	2–5 $\mu\text{m}$	28	—	Degradation	120
KMNRs	Magnetic	1.8	NH <sub>2</sub> -PS	1.5 $\mu\text{m}$	82–95	5	Adsorption	135
MARS	Magnetic	2–4	PS	80 nm	70–92	5	Degradation	10
PU/CD-SG microrobot	Self	150 000	PS	50 nm	—	10	Degradation	155
Sunflower pollen grains (SPGs) based micromotors	Self	104	PS	100 $\mu\text{m}$	—	10	Conjugate $\pi$ -region and functional groups	155
Bi <sub>2</sub> WO <sub>6</sub> microrobot	Visible light	2.9	Textile fibers	~30	70–75	6	Noncontact shoveling	131
Sb <sub>2</sub> S <sub>3</sub> -Fe <sub>3</sub> O <sub>4</sub>	Magnetic and UV light	0.6–1.6	PHB, PLA	13 $\mu\text{m}$	—	—	Photocatalysis adhesion	121
BiVO <sub>4</sub> /Fe <sub>3</sub> O <sub>4</sub> microrobots	Visible light and magnetic	6	Cellulose acetate	Micro-size	—	2	Degradation	122
TiO <sub>2</sub> -SA-NT	UV light	2–3.5	PS	60–80 $\mu\text{m}$	—	—	Adsorption and precipitation	91
Fe <sub>3</sub> O <sub>4</sub> /Bi <sub>2</sub> O <sub>3</sub> /Ag microrobots	UV light	13.2	PP	4.8–5.8 $\mu\text{m}$	—	—	Photogravitaxis	123
Hydrogel actuator	Magnetic	0.5	MCPs	20 $\mu\text{m}$	—	—	Photocatalysis adhesion	168
PDA@Fe <sub>3</sub> O <sub>4</sub> MagRobots	UV light	4.34	PCL	—	94–99	—	Adsorption	124
Ion-exchange resin-based SMR	Magnetic	3–7	PS, PVC, PA, PMMA, PVDF	20–140 $\mu\text{m}$	90–99	100	Adhesive	169
	Magnetic	3–7	PS, PVC, PA, PMMA, PVDF	1–40 $\mu\text{m}$	90–99	100	Self-electrophoretic, long-range dynamic attraction and electrostatic adsorption	136
	Magnetic	3–7	PS, PVC, PA, PMMA, PVDF	200 nm	90–99	100	Photodegradation	132
Hematite/metal Janus	Magnetic and UV light	2–12	PEG	550 nm	~100	—	Photodegradation	132
Magnetic nanorobots	Magnetic	2–14	PS	—	90	—	Nile red	133
Magnetic algae robot	Magnetic	35	PS	200 nm	71–92	5	Electrostatic attraction	10
Polymeric magnetic microrobots	Magnetic	20–37	PS	1.5 $\mu\text{m}$ , 50 nm	—	3	Capturing	126
GO <sub>x</sub> /Cat	Glucose as fuel	25–125	PE	1 $\mu\text{m}$	76–80	5	High surface tension of glucose bubbles	157

**Table 2** Comparison between light-driven and magnetically driven robots considering different parameters

Category	Light-driven robots	Magnetically driven robots
Motion controlled by	UV light, visible light	Magnetic fields
Speed ( $\mu\text{m s}^{-1}$ )	0.5–65.52	1.8–104
Plastic types processed	PS, PE, PEG, PLA, PCL, PET, PP, MCPs	PS, PE, PCL, NH <sub>2</sub> -PS, PP, PVC, PA, PMMA, PVDF
Size range	500 nm–100 $\mu\text{m}$	50 nm–200 $\mu\text{m}$
Removal efficiency (%)	10–99	10–99
Number of recycles	Typically not specified, some up to 10	Up to 100
Mechanisms	Photocatalysis, electrostatic interactions, degradation, photogravitaxis, diffusiophoretic effect	Adsorption, electrostatic interactions, non-contact shoveling, enzymatic degradation, self-electrophoretic
Efficiency	High for small-scale applications but may be slower for bulk material removal	More consistent across various plastic types, faster for bulk material removal
Cost	Lower in terms of material costs, but requires light sources ( <i>e.g.</i> , UV lamps)	Higher due to reliance on external magnetic fields and control equipment
Applicable scenarios	Suitable for sunlight-exposed environments, wastewater treatment, and photocatalytic degradation applications	Deal for controlled environments, targeted plastic removal, and bulk collection
Example references	110, 111, 115, 118 and 119	124, 126–128 and 130

classifying nano- and MPs in real-time from other nonplastic particles in natural waters such as Lake Ontario and the Saint Lawrence River, with no need for sample preparation. AI-assisted nano-DIHM can identify waterborne nano/microplastics within milliseconds, distinguishing 2% and 1% of particles in these waters, respectively. This technology provides detailed physico-chemical properties of individual particles or clusters, including size, shape, optical phase, perimeter, surface area, roughness, and edge gradient. It is adept at differentiating nano/microplastics from complex mixtures of organic, inorganic, and biological particles, as well as coated heterogeneous clusters.<sup>162</sup> The AI-assisted nano-DIHM enables 4D tracking and 3D structural and spatial analysis of waterborne nano/microplastics. The data gathered by nano-DIHM has been validated through independent methods, including transmission electron microscopy, mass spectrometry, and nanoparticle tracking analysis.<sup>163</sup> Complementary modeling has demonstrated that nano- and microplastics exhibit significantly different distribution patterns in water, influencing their transport and fate, making nano-DIHM an invaluable tool for accurate life-cycle analysis of these pollutants and identifying hotspots for remediation.<sup>164,165</sup>

Additionally, Lubongo *et al.*<sup>166</sup> highlighted the importance of automated sorting equipment enhanced by spectroscopic methods for identifying plastic types. They also discussed the fundamental principles of machine learning (ML) and AI, emphasizing their integration with spectroscopy, which is central to modern sorting technologies. The different kinds of robots those were used in the literature are summarized in Table 1 along with various features. Moreover, a comparison between light-driven and magnetically driven robots is presented in Table 2.

## 4. Conclusions and future challenges

Robots, whether operating autonomously or under human guidance, are machines designed to carry out specific tasks.

Among these, small-scale robots, often smaller than 100 micrometers, originally termed “micro- and nanomotors,” represent micro- and nanostructured materials that can harness energy from their environment and convert it into motion. These minute devices excel due to the interplay between their dynamic movement and their distinct size-, shape-, and structure-dependent physicochemical properties at the micro- and nanoscale. This synergy grants them superior performance over passive materials such as conventional static micro- and nanomaterials especially in applications like water remediation. The active motion of micro- and nanomotors induces fluid movement around them, significantly enhancing the mass transfer of chemical reactions, which, in static systems, relies solely on passive diffusion. This dynamic interaction between the motors and water contaminants leads to quicker purification processes. As the need for more complex functions arose—such as targeting specific plastic pollutants or coordinating the robots to work collectively for enhanced removal and degradation efficiency the design of micro- and nanomotors became increasingly sophisticated. The integration of propulsion mechanisms, multifunctional capabilities, environmental adaptability, collective behaviors, and intercommunication has evolved these materials into what are now known as intelligent micro- and nanorobots. Achieving self-propulsion in these tiny robots requires precise fabrication techniques to create asymmetry in their structures, enabling them to disrupt the symmetry of their surrounding field and move effectively. Based on their propulsion mechanisms, micro- and nanorobots can be categorized into fuel-driven and externally driven types. This review delves into the advanced technologies, including robotic and AI-enhanced methods that are currently being used to remove, collect, and analyze MNPs. It presents a comprehensive framework that integrates efforts across the stages of collecting, processing, and characterizing these pollutants. Additionally, the review highlights emerging robotic and machine learning technologies aimed at promoting research and solutions to combat plastic pollution effectively.

Despite the promising potential of robots for plastic removal, several challenges and limitations must be addressed to fully realize their capabilities. One of the primary challenges for robotic technologies lies in their operational scalability and efficiency in real-world conditions. Developing durable and reliable robots that can withstand harsh environmental conditions, such as strong currents, waves, and extreme temperatures, is a significant technical challenge. For example, light-powered robots may face limitations in efficiency due to fluctuating light availability, while heat- and electricity-powered systems may demand complex infrastructure and present safety concerns. Additionally, deploying robotic systems in diverse environmental conditions, such as deep-sea or extreme weather, often requires specialized and costly adaptations, which can hinder widespread adoption. Maintenance and repair in these scenarios also add to the operational challenges. Ensuring that robots have sufficient power supply and battery life for extended operations is also crucial for their effectiveness. While robots are designed to mitigate plastic pollution, their deployment must not create additional environmental problems. This includes ensuring that the materials used in robot construction are environmentally friendly and that robots do not inadvertently harm marine life or ecosystems during their operations. The cost of developing, deploying, and maintaining robotic systems can be high. Securing funding and resources for large-scale robotic cleanup projects can be challenging, particularly in regions with limited financial capabilities. Cost-effective solutions and funding models are necessary to support the widespread adoption of robotic technologies for plastic removal. Furthermore, the deployment of robots for plastic removal must comply with existing regulations and guidelines to ensure environmental and public safety. Ethical considerations, such as the impact on local communities and potential job displacement, must also be addressed to promote the responsible use of robotic technologies. Another shared limitation is the potential for unintended environmental impacts. Smart materials, if not designed and managed carefully, could contribute to secondary pollution or disrupt ecosystems. Furthermore, the long-term durability and recyclability of many smart materials remain uncertain, raising questions about their overall sustainability. Smart materials may also face difficulties in effectively targeting or isolating specific types of plastic waste in heterogeneous environments, which can reduce their efficiency.

The future of robotic strategies for plastic removal holds great promise, driven by continuous research and development efforts to address existing challenges and enhance system capabilities. As advancements in technology progress, robotic systems are expected to become more efficient, adaptable, and effective in tackling plastic pollution. Future innovations may include improved propulsion methods, more sophisticated sensing and navigation capabilities, and advanced materials that enhance the performance and longevity of these robots. Continued advancements in AI, machine learning, sensor technologies, and materials science will lead to more sophisticated and efficient robots for plastic removal. Innovations such as improved object recognition algorithms, more durable and lightweight materials, and advanced energy storage solutions

will enhance the performance and reliability of robotic systems. Robotic technologies can be integrated with other waste management systems, such as recycling and waste-to-energy facilities, to create a comprehensive approach to plastic pollution. This integration can optimize the entire lifecycle of plastic waste, from collection to processing and recycling, ensuring that plastic waste is managed sustainably. The regulatory bodies play a vital part in stimulating the approval of robotic tools for plastic removal. Policies that incentivize research and development, provide funding for robotic cleanup projects, and establish guidelines for the responsible use of robots will support the growth of this innovative field. Collaboration between governments, non-governmental organizations, industry stakeholders, and local communities is essential for the successful implementation of robotic strategies for plastic removal. Global initiatives and partnerships can facilitate knowledge sharing, resource mobilization, and coordinated efforts to address plastic pollution on a larger scale.

## Data availability

The data supporting the findings of this review are derived from publicly available sources, including peer-reviewed journals, research articles, and industry reports. No new datasets were created or analyzed during the preparation of this review. All relevant data can be accessed through the referenced publications, which are cited throughout the manuscript. For further information or specific data requests, please refer to the respective sources or contact the authors directly.

## Conflicts of interest

The authors declare that they have no identifiable financial conflicts of interest or personal connections that could have influenced the findings presented in this study.

## Acknowledgements

The authors express their gratitude to the National Natural Science Foundation of China (no. W243305) and the Funding of Wuhan Textile University (no. 2023508 and 2024015) for their vital support.

## References

- 1 S. Freinkel, *Plastic: a toxic love story*, HMH, 2011.
- 2 N. Singh, D. Hui, R. Singh, I. Ahuja, L. Feo and F. Fraternali, *Composites, Part B*, 2017, **115**, 409–422.
- 3 J. Mercelis, *Beyond Bakelite: Leo Baekeland and the business of science and invention*, MIT Press, 2020.
- 4 C. Martin, F. Baalkhuyur, L. Valluzzi, V. Saderne, M. Cusack, H. Almahasheer, P. Krishnakumar, L. Rabaoui, M. Qurban and A. Arias-Ortiz, *Sci. Adv.*, 2020, **6**, eaaz5593.
- 5 K. Ugoeze, E. Amogu, K. Oluigbo and N. Nwachukwu, *J. Environ. Sci. Public Health.*, 2021, **5**, 1–31.



- 6 R. Geyer, *Plastic waste and recycling*, Elsevier, 2020, pp. 13–32.
- 7 O. O. Ayeleru, S. Dlova, O. J. Akinribide, F. Ntuli, W. K. Kupolati, P. F. Marina, A. Blencowe and P. A. Olubambi, *Waste Manage.*, 2020, **110**, 24–42.
- 8 R. Molenaar, S. Chatterjee, B. Kamphuis, I. M. Segers-Nolten, M. M. Claessens and C. Blum, *Environ. Sci.: Nano*, 2021, **8**, 723–730.
- 9 L. Rahman, G. Mallach, R. Kulka and S. Halappanavar, *Nanotoxicology*, 2021, **15**, 1253–1278.
- 10 X. Peng, M. Urso, M. Kolackova, D. Huska and M. Pumera, *Adv. Funct. Mater.*, 2024, **34**, 2307477.
- 11 M. Urso and M. Pumera, *Adv. Funct. Mater.*, 2022, **32**, 2112120.
- 12 P. Guo, Y. Wang, P. Moghaddamfard, W. Meng, S. Wu and Y. Bao, *J. Hazard. Mater.*, 2024, 134405.
- 13 W. Liu, H. Liao, M. Wei, M. Junaid, G. Chen and J. Wang, *TrAC, Trends Anal. Chem.*, 2023, 117477.
- 14 W. Li, J. Wang, Z. Xiong and D. Li, *Cell Rep. Phys. Sci.*, 2023, **4**.
- 15 P. Li and J. Liu, *Environ. Sci. Technol.*, 2024, **58**, 3065–3078.
- 16 S. Wen, Y. Zhao, M. Wang, H. Yuan and H. Xu, *Crit. Rev. Food Sci. Nutr.*, 2024, **64**, 1429–1447.
- 17 M. R. Abbing, *Plastic soup: an atlas of ocean pollution*, Island Press, 2019.
- 18 N. Gupta, T. Parsai and H. V. Kulkarni, *J. Environ. Manage.*, 2024, **350**, 119559.
- 19 M. Urso, M. Ussia and M. Pumera, *Nat. Rev. Bioeng.*, 2023, **1**, 236–251.
- 20 V. Kumar, E. Singh, S. Singh, A. Pandey and P. C. Bhargava, *Chem. Eng. J.*, 2023, **459**, 141568.
- 21 C. Su, *J. Hazard. Mater.*, 2017, **322**, 48–84.
- 22 A. Saravanan, P. S. Kumar, S. Jeevanantham, S. Karishma, B. Tajsabreen, P. Yaashikaa and B. Reshma, *Chemosphere*, 2021, **280**, 130595.
- 23 A. Kundu, N. P. Shetti, S. Basu, K. R. Reddy, M. N. Nadagouda and T. M. Aminabhavi, *Chem. Eng. J.*, 2021, **421**, 129816.
- 24 Q. Liu, Y. Chen, Z. Chen, F. Yang, Y. Xie and W. Yao, *Sci. Total Environ.*, 2022, **851**, 157991.
- 25 Z. Chen, X. Liu, W. Wei, H. Chen and B.-J. Ni, *Water Res.*, 2022, **221**, 118820.
- 26 B. Mohan, K. Singh, R. K. Gupta, A. Kumar, A. J. Pombeiro and P. Ren, *Sep. Purif. Technol.*, 2024, 126987.
- 27 C. Y. Teh, P. M. Budiman, K. P. Y. Shak and T. Y. Wu, *Ind. Eng. Chem. Res.*, 2016, **55**, 4363–4389.
- 28 M. Shen, B. Song, G. Zeng, Y. Zhang, W. Huang, X. Wen and W. Tang, *Environ. Pollut.*, 2020, **263**, 114469.
- 29 V. Lynn and K. Cooley, *Nanorobotics*, Scientific e-Resources, 2018.
- 30 Z. Chen, W. Si, V. C. Johnson, S. A. Oke, S. Wang, X. Lv, M. L. Tan, F. Zhang and X. Ma, *J. Environ. Manage.*, 2025, **373**, 123815.
- 31 J. Wang, Y. Dong, P. Ma, Y. Wang, F. Zhang, B. Cai, P. Chen and B. F. Liu, *Adv. Mater.*, 2022, **34**, 2201051.
- 32 L. Kong, J. Guan and M. Pumera, *Curr. Opin. Electrochem.*, 2018, **10**, 174–182.
- 33 X. Liu, Y. Jing, C. Xu, X. Wang, X. Xie, Y. Zhu, L. Dai, H. Wang, L. Wang and S. Yu, *Nanomaterials*, 2023, **13**, 2872.
- 34 W. Li, Y. Yin, H. Zhou, Y. Fan, Y. Yang, Q. Gao, P. Li, G. Gao and J. Li, *Cyborg Bionic Syst.*, 2024, **5**, 0101.
- 35 H. Zheng, S. Huang, J. Huang, H. Zeng, M. Xu, A. Cai, S. Zhou, X. Ma and J. Deng, *J. Hazard. Mater.*, 2024, **480**, 136440.
- 36 Y. Ju, R. Hu, Y. Xie, J. Yao, X. Li, Y. Lv, X. Han, Q. Cao and L. Li, *Nano Energy*, 2021, **87**, 106169.
- 37 Z. Ren and M. Sitti, *Nat. Protoc.*, 2024, **19**, 441–486.
- 38 K. Moriyama, S. Nakao, M. Tsuji, N. Nakagawa, T. Satake and Y. Johnno, *Biochem. Eng. J.*, 2024, **208**, 109338.
- 39 S. Nocentini, C. Parmeggiani, D. Martella and D. S. Wiersma, *Adv. Opt. Mater.*, 2018, **6**, 1800207.
- 40 S. Lim, Y. Du, Y. Lee, S. K. Panda, D. Tong and M. K. Jawed, *Bioinspiration Biomimetics*, 2022, **18**, 011003.
- 41 J. Li, B. Esteban-Fernández de Ávila, W. Gao, L. Zhang and J. Wang, *Sci. Robot.*, 2017, **2**, eaam6431.
- 42 G. Zhang, R. Ren, X. Yan, H. Zhang and Y. Zhu, *Ecotoxicol. Environ. Saf.*, 2024, **287**, 117235.
- 43 A. Elnaggar, S. Kang, M. Tian, B. Han and M. Keshavarz, *Small Sci.*, 2024, **4**, 2300211.
- 44 L. Wang, Z. Meng, Y. Chen and Y. Zheng, *Adv. Intell. Syst.*, 2021, **3**, 2000267.
- 45 S. Pané, J. Puigmartí-Luis, C. Bergeles, X. Z. Chen, E. Pellicer, J. Sort, V. Počepcová, A. Ferreira and B. J. Nelson, *Adv. Mater. Technol.*, 2019, **4**, 1800575.
- 46 X. Wu, X. Peng, L. Ren, J. Guan and M. Pumera, *Adv. Funct. Mater.*, 2024, 2410167.
- 47 S. Preetam, *Nanoscale Adv.*, 2024, **6**, 2569–2581.
- 48 M. Shen, H. Li, T. Hu, W. Wang, K. Zheng and H. Zhang, *Sci. Total Environ.*, 2024, 175153.
- 49 F. Glaviano, R. Esposito, A. D. Cosmo, F. Esposito, L. Gerevini, A. Ria, M. Molinara, P. Bruschi, M. Costantini and V. Zupo, *J. Mar. Sci. Eng.*, 2022, **10**, 297.
- 50 E. Schmaltz, E. C. Melvin, Z. Diana, E. F. Gunady, D. Rittschof, J. A. Somarelli, J. Virdin and M. M. Dunphy-Daly, *Environ. Int.*, 2020, **144**, 106067.
- 51 Y. Chen, C. Valenzuela, X. Zhang, X. Yang, L. Wang and W. Feng, *Nat. Commun.*, 2023, **14**, 3036.
- 52 M. Zeng, M. Chen, D. Huang, S. Lei, X. Zhang, L. Wang and Z. Cheng, *Mater. Horiz.*, 2021, **8**, 758–802.
- 53 L. Hines, K. Petersen, G. Z. Lum and M. Sitti, *Adv. Mater.*, 2017, **29**, 1603483.
- 54 M. Li, A. Pal, A. Aghakhani, A. Pena-Francesch and M. Sitti, *Nat. Rev. Mater.*, 2022, **7**, 235–249.
- 55 A. Miriyev, K. Stack and H. Lipson, *Nat. Commun.*, 2017, **8**, 596.
- 56 A. L. P. Silva, *Curr. Opin. Green Sustainable Chem.*, 2021, **28**, 100443.
- 57 B. Jorgensen, M. Krasny and J. Baztan, *Sustainability Sci.*, 2021, **16**, 153–167.
- 58 S. Lucrezi and O. Digun-Aweto, *Mar. Pollut. Bull.*, 2020, **155**, 111167.
- 59 A. Feil, T. Pretz, M. Jansen and E. U. Thoden van Velzen, *Waste Manage. Res.*, 2017, **35**, 172–180.
- 60 O. K. Helinski, C. J. Poor and J. M. Wolfand, *Mar. Pollut. Bull.*, 2021, **165**, 112095.

- 61 J. van Stijn, 2023.
- 62 M. G. Kibria, N. I. Masuk, R. Safayet, H. Q. Nguyen and M. Mourshed, *Int. J. Environ. Res.*, 2023, **17**, 20.
- 63 C. Axelsson and E. van Seville, *Mar. Pollut. Bull.*, 2017, **124**, 211–227.
- 64 P. Kershaw, S. Katsuhiko, S. Lee and D. Woodring, United Nations Environment Programme, 2011.
- 65 M. Simon, A. Vianello and J. Vollertsen, *Water*, 2019, **11**, 1935.
- 66 Y.-J. Chen, Y. Chen, C. Miao, Y.-R. Wang, G.-K. Gao, R.-X. Yang, H.-J. Zhu, J.-H. Wang, S.-L. Li and Y.-Q. Lan, *J. Mater. Chem. A*, 2020, **8**, 14644–14652.
- 67 X. Shi, X. Zhang, W. Gao, Y. Zhang and D. He, *Sci. Total Environ.*, 2022, **802**, 149838.
- 68 A. Batool and S. Valiyaveetil, *ACS Sustainable Chem. Eng.*, 2020, **8**, 13481–13487.
- 69 C. E. Enyoh, O. O. Fadare, M. Paredes, Q. Wang, A. W. Verla, L. Shafea and T. Chowdhury, *Microplastics Pollution in Aquatic Media: Occurrence, Detection, and Removal*, 2022, pp. 273–289.
- 70 M. Shen, G. Zeng, Y. Zhang, X. Wen, B. Song and W. Tang, *Sci. Total Environ.*, 2019, **697**, 134200.
- 71 C. Akarsu, H. Kumbur and A. E. Kideys, *Water Sci. Technol.*, 2021, **84**, 1648–1662.
- 72 M. Babalar, S. Siddiqua and M. A. Sakr, *Sep. Purif. Technol.*, 2024, **331**, 125582.
- 73 T. Maes, R. Jessop, N. Wellner, K. Haupt and A. G. Mayes, *Sci. Rep.*, 2017, **7**, 44501.
- 74 J. Talvitie, A. Mikola, A. Koistinen and O. Setälä, *Water Res.*, 2017, **123**, 401–407.
- 75 P. Gupta and R. Kaushik, *Soft Computing in Smart Manufacturing and Materials*, Elsevier, 2025, pp. 47–74.
- 76 J. R. Regalbuto, *Synthesis of Solid Catalysts*, 2009, pp. 33–58.
- 77 H. Yu, B. Yang, M. G. Waigi, F. Peng, Z. Li and X. Hu, *Chemosphere*, 2020, **261**, 127592.
- 78 A. Misra, C. Zambrzycki, G. Kloker, A. Kotyrba, M. H. Anjass, I. Franco Castillo, S. G. Mitchell, R. Güttel and C. Streb, *Angew. Chem., Int. Ed.*, 2020, **59**, 1601–1605.
- 79 K. Rajala, O. Grönfors, M. Hesampour and A. Mikola, *Water Res.*, 2020, **183**, 116045.
- 80 M. Prokopova, K. Novotna, L. Pivokonska, L. Cermakova, T. Cajthaml and M. Pivokonsky, *J. Environ. Chem. Eng.*, 2021, **9**, 106465.
- 81 C. Li, R. Busquets, R. B. Moruzzi and L. C. Campos, *J. Water Process Eng.*, 2021, **44**, 102346.
- 82 H. Ermis, C. Collins, S. K. Saha and P. Murray, *Chem. Eng. J.*, 2024, 154585.
- 83 C. O. Adetunji and O. A. Anani, *Microbial Rejuvenation of Polluted Environment*, 2021, vol. 1, pp. 353–372.
- 84 Y. Yang, J. Yang, W.-M. Wu, J. Zhao, Y. Song, L. Gao, R. Yang and L. Jiang, *Environ. Sci. Technol.*, 2015, **49**, 12080–12086.
- 85 A. L. Dawson, S. Kawaguchi, C. K. King, K. A. Townsend, R. King, W. M. Huston and S. M. Bengtson Nash, *Nat. Commun.*, 2018, **9**, 1001.
- 86 S. Yoshida, K. Hiraga, T. Takehana, I. Taniguchi, H. Yamaji, Y. Maeda, K. Toyohara, K. Miyamoto, Y. Kimura and K. Oda, *Science*, 2016, **351**, 1196–1199.
- 87 S. Ügdüler, K. M. Van Geem, M. Roosen, E. I. Delbeke and S. De Meester, *Waste Manage.*, 2020, **104**, 148–182.
- 88 L. Wang, W.-M. Wu, N. S. Bolan, D. C. Tsang, Y. Li, M. Qin and D. Hou, *J. Hazard. Mater.*, 2021, **401**, 123415.
- 89 R. A. Brooks, *Science*, 1991, **253**, 1227–1232.
- 90 H. Muaddi, M. El Hafid, W. J. Choi, E. Lillie, C. de Mestral, A. Nathens, T. A. Stukel and P. J. Karanicolas, *Ann. Surg.*, 2021, **273**, 467–473.
- 91 S. M. Beladi-Mousavi, S. Hermanova, Y. Ying, J. Plutnar and M. Pumera, *ACS Appl. Mater. Interfaces*, 2021, **13**, 25102–25110.
- 92 F. Hartmann, M. Baumgartner and M. Kaltenbrunner, *Adv. Mater.*, 2021, **33**, 2004413.
- 93 C. Lubongo, M. A. B. Daej and P. Alexandridis, *Reuse of Plastic Waste in Eco-Efficient Concrete*, Elsevier, 2024, pp. 13–35.
- 94 C. Lubongo and P. Alexandridis, *Recycling*, 2022, **7**, 11.
- 95 C. Conway and A. Gaynullin, 2022.
- 96 J. Falk-Andersson, M. L. Haarr and V. Havas, *Sci. Total Environ.*, 2020, **745**, 141117.
- 97 A. R. Frey, 2024.
- 98 A. Chidepatil, P. Bindra, D. Kulkarni, M. Qazi, M. Kshirsagar and K. Sankaran, *Adm. Sci.*, 2020, **10**, 23.
- 99 I. Cortesi, A. Masiero, G. Tucci and K. Topouzelis, *The International Archives of the Photogrammetry, Remote Sensing and Spatial Information Sciences*, 2022, vol. 43, pp. 855–861.
- 100 L. Goddijn-Murphy, B. J. Williamson, J. McIlvenny and P. Corradi, *Remote Sens.*, 2022, **14**, 3179.
- 101 S. i Kako, S. Morita and T. Taneda, *Mar. Pollut. Bull.*, 2020, **155**, 111127.
- 102 J. Rojas, 2018.
- 103 N. Rupavathi, A. Dhineshkumar, G. Manokar and D. Vasanthakumar, *Int. Res. J. Innov. Eng. Technol.*, 2024, **8**, 213.
- 104 J. Wang, *Nanomachines: fundamentals and applications*, John Wiley & Sons, 2013.
- 105 C. Li, Y. Xu, W. Tu, G. Chen and R. Xu, *Green Chem.*, 2017, **19**, 882–899.
- 106 S. Chu, B. Zhang, X. Zhao, H. S. Soo, F. Wang, R. Xiao and H. Zhang, *Adv. Energy Mater.*, 2022, **12**, 2200435.
- 107 J. Ge, Z. Zhang, Z. Ouyang, M. Shang, P. Liu, H. Li and X. Guo, *Environ. Res.*, 2022, **209**, 112729.
- 108 J. He, L. Han, F. Wang, C. Ma, Y. Cai, W. Ma, E. G. Xu, B. Xing and Z. Yang, *Crit. Rev. Environ. Sci. Technol.*, 2023, **53**, 504–526.
- 109 Z. Yang, Y. Li and G. Zhang, *Chemosphere*, 2024, 141939.
- 110 H. Wang, Y. Jing, J. Yu, B. Ma, M. Sui, Y. Zhu, L. Dai, S. Yu, M. Li and L. Wang, *Front. Bioeng. Biotechnol.*, 2023, **11**, 1312074.
- 111 X. Peng, M. Urso, M. Ussia and M. Pumera, *ACS Nano*, 2022, **16**, 7615–7625.
- 112 Q. Zhang, R. Dong, Y. Wu, W. Gao, Z. He and B. Ren, *ACS Appl. Mater. Interfaces*, 2017, **9**, 4674–4683.
- 113 J. Simmchen, A. Baeza, A. Miguel-Lopez, M. M. Stanton, M. Vallet-Regi, D. Ruiz-Molina and S. Sánchez, *ChemNano-Mat*, 2017, **3**, 65–71.

- 114 J. Palacci, S. Sacanna, A. Vatchinsky, P. M. Chaikin and D. J. Pine, *J. Am. Chem. Soc.*, 2013, **135**, 15978–15981.
- 115 K. Villa, F. Novotný, J. Zelenka, M. P. Browne, T. S. Ruml and M. Pumera, *ACS Nano*, 2019, **13**, 8135–8145.
- 116 S. G. Ullattil and M. Pumera, *Small*, 2023, **19**, 2301467.
- 117 L. Wang, A. Kaeppler, D. Fischer and J. Simmchen, *ACS Appl. Mater. Interfaces*, 2019, **11**, 32937–32944.
- 118 P. Mayorga-Burrezo, C. C. Mayorga-Martinez and M. Pumera, *J. Colloid Interface Sci.*, 2023, **643**, 447–454.
- 119 M. Urso, M. Ussia, F. Novotný and M. Pumera, *Nat. Commun.*, 2022, **13**, 3573.
- 120 P. Chattopadhyay, M. C. Ariza-Tarazona, E. I. Cedillo-González, C. Siligardi and J. Simmchen, *Nanoscale*, 2023, **15**, 14774–14781.
- 121 K. Villa, L. Děkanovský, J. Plutnar, J. Kosina and M. Pumera, *Adv. Funct. Mater.*, 2020, **30**, 2007073.
- 122 A. Jancik-Prochazkova, V. Jašek, S. Figalla and M. Pumera, *Adv. Opt. Mater.*, 2023, **11**, 2300782.
- 123 A. Jancik-Prochazkova, H. Kmentova, X. Ju, S. Kment, R. Zboril and M. Pumera, *Adv. Funct. Mater.*, 2024, 2402567.
- 124 Q. Guo, Y. Liu, J. Liu, Y. Wang, Q. Cui, P. Song, X. Zhang and C. Zhang, *Chem. Mater.*, 2022, **34**, 5165–5175.
- 125 A. I. Bunea, D. Martella, S. Nocentini, C. Parmeggiani, R. Taboryski and D. S. Wiersma, *Adv. Intell. Syst.*, 2021, **3**, 2000256.
- 126 M. Ussia, M. Urso, C. M. Oral, X. Peng and M. Pumera, *ACS Nano*, 2024, **18**, 13171–13183.
- 127 S. Kim, F. Qiu, S. Kim, A. Ghanbari, C. Moon, L. Zhang, B. J. Nelson and H. Choi, *Adv. Mater.*, 2013, **25**, 5863–5868.
- 128 E. Diller, J. Giltinan and M. Sitti, *Int. J. Robot. Res.*, 2013, **32**, 614–631.
- 129 C. C. Alcántara, S. Kim, S. Lee, B. Jang, P. Thakolkaran, J. Y. Kim, H. Choi, B. J. Nelson and S. Pané, *Small*, 2019, **15**, 1805006.
- 130 R. Maria-Hormigos, C. C. Mayorga-Martinez and M. Pumera, *Small Methods*, 2023, **7**, 2201014.
- 131 M. Sun, W. Chen, X. Fan, C. Tian, L. Sun and H. Xie, *Appl. Mater. Today*, 2020, **20**, 100682.
- 132 M. Urso, M. Ussia and M. Pumera, *Adv. Funct. Mater.*, 2021, **31**, 2101510.
- 133 D. I. Velikov, A. Jancik-Prochazkova and M. Pumera, *ACS Nanosci. Au*, 2024, **4**, 243–249.
- 134 H. Zhou, C. C. Mayorga-Martinez and M. Pumera, *Small methods*, 2021, **5**, 2100230.
- 135 M. Zhang, S. Yang, W. Zhong, H. Wang, U. Uthappa and B. Wang, *Chem. Eng. J.*, 2024, **495**, 153264.
- 136 W. Li, C. Wu, Z. Xiong, C. Liang, Z. Li, B. Liu, Q. Cao, J. Wang, J. Tang and D. Li, *Sci. Adv.*, 2022, **8**, eade1731.
- 137 L. Soler and S. Sánchez, *Nanoscale*, 2014, **6**, 7175–7182.
- 138 W. Chen, Y. Song, Y. Liu, J. Chen and X. Ma, 2024.
- 139 L. Tang, Y. Liu, J. Wang, G. Zeng, Y. Deng, H. Dong, H. Feng, J. Wang and B. Peng, *Appl. Catal., B*, 2018, **231**, 1–10.
- 140 K. M. Shah, I. H. Billinge, X. Chen, H. Fan, Y. Huang, R. K. Winton and N. Y. Yip, *Desalination*, 2022, **538**, 115827.
- 141 U. Diaz, D. Brunel and A. Corma, *Chem. Soc. Rev.*, 2013, **42**, 4083–4097.
- 142 N. Vedachalam, R. Ramesh, V. B. N. Jyothi, V. Doss Prakash and G. Ramadass, *Mar. Georesour. Geotechnol.*, 2019, **37**, 525–538.
- 143 M. Mathesh, J. Sun and D. A. Wilson, *J. Mater. Chem. B*, 2020, **8**, 7319–7334.
- 144 J. Li, I. Rozen and J. Wang, *ACS Nano*, 2016, **10**, 5619–5634.
- 145 Q. Yang, Y. Gao, L. Xu, W. Hong, Y. She and G. Yang, *Int. J. Biol. Macromol.*, 2021, **167**, 457–469.
- 146 K. Liu, J. Ou, S. Wang, J. Gao, L. Liu, Y. Ye, D. A. Wilson, Y. Hu, F. Peng and Y. Tu, *Appl. Mater. Today*, 2020, **20**, 100694.
- 147 H. Ye, Y. Wang, X. Liu, D. Xu, H. Yuan, H. Sun, S. Wang and X. Ma, *J. Colloid Interface Sci.*, 2021, **588**, 510–521.
- 148 M. Zeng, S. Yuan, D. Huang and Z. Cheng, *ACS Appl. Mater. Interfaces*, 2019, **11**, 40099–40106.
- 149 K. Villa, J. Parmar, D. Vilela and S. Sánchez, *ACS Appl. Mater. Interfaces*, 2018, **10**, 20478–20486.
- 150 R. Niu, E. C. Oğuz, H. Müller, A. Reinmüller, D. Botin, H. Löwen and T. Palberg, *Phys. Chem. Chem. Phys.*, 2017, **19**, 3104–3114.
- 151 N. Ran, B. Denis, W. Julian, R. L. Alexander and P. Thomas, 2017.
- 152 R. Niu and T. Palberg, *Soft Matter*, 2018, **14**, 3435–3442.
- 153 C. Wu, J. Dai, X. Li, L. Gao, J. Wang, J. Liu, J. Zheng, X. Zhan, J. Chen and X. Cheng, *Nat. Nanotechnol.*, 2021, **16**, 288–295.
- 154 A. Mahmud, M. M. Wasif, H. Roy, F. Mehnaz, T. Ahmed, M. N. Pervez, V. Naddeo and M. S. Islam, *Water*, 2022, **14**, 3968.
- 155 Y. Wang, G. Su, J. Li, Q. Guo, Y. Miao and X. Zhang, *Nano Lett.*, 2022, **22**, 5409–5419.
- 156 Z. Huang, Q. Cui, X. Yang, F. Wang and X. Zhang, *J. Hazard. Mater.*, 2023, **446**, 130673.
- 157 H. G. V. Ho and P. J. Yoo, *Sep. Purif. Technol.*, 2024, **351**, 127952.
- 158 J. Kang, L. Zhou, X. Duan, H. Sun, Z. Ao and S. Wang, *Matter*, 2019, **1**, 745–758.
- 159 M. Umebara, N. Sugai, K. Murayama, T. Sugawara, Y. Akashi, Y. Morita, R. Kato and T. Komatsu, *Mater. Adv.*, 2021, **2**, 6428–6438.
- 160 D. Vilela, J. Parmar, Y. Zeng, Y. Zhao and S. Sánchez, *Nano Lett.*, 2016, **16**, 2860–2866.
- 161 Z. Wang, D. Pal, A. Pilechi and P. A. Ariya, *Environ. Sci. Technol.*, 2024, **58**, 8919–8931.
- 162 D. M. Mitrano, P. Wick and B. Nowack, *Nat. Nanotechnol.*, 2021, **16**, 491–500.
- 163 L. D. Mandemaker and F. Meirer, *Angew. Chem., Int. Ed.*, 2023, **62**, e202210494.
- 164 D. Calore and N. Fraticelli, *Microplastics*, 2022, **1**, 640–650.
- 165 S. Vohl, M. Kristl and J. Stergar, *Nanomaterials*, 2024, **14**, 1179.
- 166 C. Lubongo, M. A. Bin Daej and P. Alexandridis, *Recycling*, 2024, **9**, 59.
- 167 S. Won, H. E. Lee, Y. S. Cho, K. Yang, J. E. Park, S. J. Yang and J. J. Wie, *Nat. Commun.*, 2022, **13**, 6750.
- 168 J. Kim, C. C. Mayorga-Martinez and M. Pumera, *Nat. Commun.*, 2023, **14**, 935.
- 169 H. Zhou, C. Mayorga-Martinez and M. Pumera, *Chem. Rev.*, 2021, **121**(8), 4999–5041.